OPTICAL AND ELECTRICAL PROPERTIES OF α-MONOCLINIC SELENIUM

Thesis by

John Caywood

In Partial Fulfillment of the Requirements

For the Degree of

Doctor of Philosophy

California Institute of Technology

Pasadena, California

1969

(Submitted May 6, 1969)

ABSTRACT

The optical absorption of α-monoclinic selenium has been measured over the range in wavelength 1.15μ to 0.2775μ. The data show a well defined absorption edge at 2.25 eV with further structure appearing as changes in $d\alpha/dE$ at 2.85 eV and 3.75 eV. For comparison the absorption of selenium in solutions in which it is believed to exist in the same eight-membered puckered ring as in the crystal was measured. This absorption is qualitatively different from that of the crystal.

The existence of surface barriers on α-monoclinic selenium crystals has been demonstrated. Photometric measurements indicate electron barrier heights of 1.05 eV and 1.3 eV, respectively, for Ga and Au contacts. The mobilities of holes and electrons have been measured by a time-of-flight technique to be about 0.2 cm^2/ V-sec and 1.6 cm^2 /V-sec, respectively, at room temperature. The hole mobility was found to be limited by traps 0.23 ± .01 eV above the valence levels, while the electron mobility is an intrinsic mobility limited only by scattering. It was found that in the region of low carrier density (i.e. no space charge effects) the number of carriers which crossed the sample was determined by the interplay of the applied field (carrying carriers across the sample) and diffusion (carrying carriers into the metal contact where they relax). The dielectric constant, K, was determined to be 9.2 ± .6 over the range 100 kH_z to 100 MH_z.

ACKNOWLEDGMENTS

I wish to thank Dr. Carver Mead for his guidance and encouragement throughout the course of this work. I also wish to especially thank Mr. Joseph Taynai, without whose patient work at crystal growth this work would not have been possible. Thanks are due Messrs. Thomas McGill and Stephen Kurtin and Drs. Marc Nicolet, Seymour Geller, James Mayer and Mark Tabak for helpful discussion and suggestions. Finally, fellowship assistance from the Ford Foundation, Fairchild Camera and Instrument Corp., and the State of California, as well as research support from ONR and JPL are gratefully acknowledged.

TABLE OF CONTENTS

GENERAL INTRODUCTION

The α-monoclinic form of selenium consists of molecules of selenium which have the form of an eight-membered puckered ring. These molecules are arranged in a crystal which has four molecules per unit cell. This form was apparently first produced by Mitscherlich in 1855.[1] Later crystallographic studies were conducted by Muthmann,[2] in 1890, and by Saunders,[3] in 1900. The electrical and optical properties were first investigated by a group at Göttingen who, in 1926, reported measurements of index of refraction, dielectric constant, and photoconductivity.[4,5] Despite the incompleteness of these investigations - for example, index of refraction and dielectric constant were each measured at only one frequency - no further work was done on the electrical or optical properties for over thirty years until Prosser measured the optical constants in the region of the long wavelength side of the absorption edge (.876-.592μ).[6] In this interregnum of 34 years, the only reported work on α-monoclinic selenium was the x-ray determination of its crystal structure by Burbank in 1950.[7] Capitalizing on Gudden and Pohl's discovery of mobile holes and electrons,[5] Spear verified the mobility of carriers of both kinds and measured the mobility of electrons over a wide temperature range.[8]

The investigation reported here extends measurements into new areas in an attempt to provide a basis for thorough understanding of this material. This thesis is divided into two parts. The first part

contains the results of measurement of optical absorption in both the α-monoclinic crystal and certain solvents in which the Se_8 ring is believed to exist. The second part concerns itself with the processes involved in a charge carrier entering a crystal from a metallic contact and moving across the crystal under the influence of an external field.

PART I

Introduction

In order to investigate the structure of the excited states one would like to extend the measurements of Prosser to considerably shorter wavelengths. A technique has been developed to grow extremely thin platelets of α-monoclinic selenium which has allowed us to extend these measurements. To compare the optical absorption processes of a molecule in the crystalline environment (in which it might be considerably perturbed by the surrounding selenium molecules) with that of a molecule in a less perturbed condition, the optical absorption of selenium dissolved in various solvents in which it is believed to exist primarily as Se_8 molecules was also measured.

CHAPTER I

α-monoclinic Crystals

1.1 Sample preparation

Small platelets of α-monoclinic Se were grown on quartz optical windows by controlled evaporation of a saturated solution of CS_2. The selenium solute was 99.99% pure while the CS_2 was reagent quality. From the numerous platelets grown on the window several were chosen. These crystals were chosen because they were large (typical dimension of 200μ), of uniform shape and of uniform thickness as determined by interference-contrast microscopy. Measurement of the angles formed by the edges of these platelets showed that the platelets correspond to

those of the (101) face of the α-monoclinic crystal, as determined by Burbank, to within better than 10 minutes of arc.[7,9] Figure 1 shows a crystal which is typical of those used in these investigations. Finally, an aluminum foil mask through which a hole of 100μ diameter had been drilled was cemented over the platelet to define the light path through the crystal.

1.2 Experimental Apparatus and Procedure

The monochromatic beam was provided by passing the light from the source through a Spex model 1400-11 double spectrometer using 600 line per mm gratings blazed at 5000 Å. Because this is a grating-type instrument care must be taken to avoid second (and higher) order radiation. This difficulty was avoided by employing as detectors vacuum photodiodes which had appreciable response only over an octave in wavelength.

In this apparatus the light from the source was chopped, passed through the monochromater, focussed onto the sample assembly by a 90° off-axis paraboloid, front surfaced, reducing mirror, and detected by the aforementioned photodiode. The output of the photodiode was amplified, demodulated by a PAR model HR-8 phase lock amplifier and read from a digital voltmeter. For calibration purposes similar measurements were made using a similar mask cemented to a clean quartz window.

After the transmission measurements were completed, the masks were removed, the crystals were overcoated, and the thickness of the crystals was measured using the Nomarski interferometer attachment of a Reichert microscope. To resolve the ambiguity inherent to interferometric measurement of sharp steps, measurements were made at the

Th 5351 Å line and the Na D lines. Consistency arguments were then used to unambiguously determine the thickness.

1.3 Results

With this system it was relatively easy to cover more than 3 orders of magnitude in relative transmission with good reproducibility and little scatter. Figure 2 shows a plot of every second point from a data run on sample Se04.

Figure 3 is a plot of $-(\ell n\ T)/d$ for two samples of different thickness, where T is relative transmission and d the corresponding thickness. Sample Se04 was 4102 Å ± 61 Å thick while Se09 was 1060 Å ± 48 Å thick. The errors represent the 95% confidence limits of the Student's test calculated from repeated measurements. Since the relative transmission, and not the absolute transmission, was measured, the highest transmission point of Se09 was set at unity and the level of Se04 was chosen to fit the two curves in the region of high absorption where reflections are unimportant. It can be seen that the fit is quite good throughout the region of high absorption. There is a well-defined change in the slope at 2.85 eV and a less well-defined change in slope around 3.75 eV. The fluctuations in the high energy region (above ~ 3.7 eV)are scatter, not structure. The measurements were extended to 1.15μ in the case of Se04, but no variations beyond those which could be attributed to interference were observed.

The planes of the Se_8 molecules are arranged approximately perpendicular to the (101) face. Since the angles formed by the edges of the (101) face differ by 4°, the orientation of molecular plane within the crystal could be determined. Measurements were made in which the

electric vector was polarized approximately parallel and perpendicular to these planes. No large difference was noted between the transmission of the crystal for polarized and unpolarized light.

CHAPTER II

Solutions

2.1 Sample Preparation and Experimental Procedure

Transmission measurements were made of 99.99% pure selenium dissolved in CS_2 , in toluene, and in trichlorethylene (TCE). The CS_2 used was reagent grade. The TCE was reagent grade which was subsequently distilled prior to use. The toluene was spectroscopic grade.

Transmission measurements employed a Cary model 14 spectrophotometer which uses a time sharing system to eliminate the effect of the solvent and container. To check this, the transmission cells were always filled with an unadulterated sample of the solvent to be employed and a transmission spectrum was taken before the solution was placed in the cell.

Concentration was determined by weighing the residue from repeated evaporations of known quantities of the solution and subtracting the weight of the residue from repeated evaporations of unadulterated solvent. The weight of the latter was always small ($<3\%$) with respect to the weight of the former.

2.2 Results

In figure 4 is plotted the atomic extinction coefficient of an approximately saturated, room temperature solution of selenium in CS_2.

Earlier workers have reported different results.[10] CS_2 begins to absorb strongly in the vicinity of 3.25 eV. It was found that because of this, special care had to be taken to obtain meaningful results in this region. The same coefficient for a solution of 1/5 of that concentration is the same to within the limits of the error bar. This demonstrates that there is no appreciable concentration effect. In addition to the random error indicated by the error bar on the graph there is a possible systematic error of ± 7% with 90% confidence from uncertainty in determination of the concentration.

Also shown in figure 4 is a plot of atomic extinction coefficient of selenium dissolved in TCE. The low solubility of selenium in TCE results in a possible systematic error from the concentration determination of ± 23% with 90% confidence for this curve. The data for toluene were qualitatively similar to that for TCE.

CHAPTER III

Discussion

3.1 Using Prosser's values[6] for n and k and equation (5) of appendix 1 to evaluate the transmission for wavelengths in the vicinity of .6μ and selenium thicknesses of .1μ one finds that the transmission of the selenium-quartz combination relative to clean quartz is about .98. This implies that the zero of the absorption constant, alpha, in figure 3, is correctly placed. Similarly evaluating eq. 5 for a sample of .4μ thickness one finds fair agreement with the baseline chosen for Se04. One can then interpret all of the change in transmission of Se09 as being due to absorption so that the curve in figure 3

does represent α as indicated. Absorption in Se04 begins at the same energy as it does in Se09, but, because of the reflection correction, has initially less effect until absorption dominates the loss whereupon the curve merges with that of Se09. Extrapolation of the linear portion of the Se09 curve to zero intercept yields an optical absorption edge of 2.25 eV at room temperature. This is in good agreement with Prosser.[6] A plot of the square root of α versus photon energy is linear over the range 2.1 eV to 2.4 eV.[4] The optical absorption may quite generally be taken to be the density of occupied lower states times the density of unoccupied upper states times the square of the matrix element for the transition between these states, integrated over the energetically allowed transitions. Thus the breaks in $d\alpha/dE$ probably represent changes in the group symmetry of either the initial and/or the final states involved in the transition.

Turning to the measurements of Se in solution one might ask what evidence exists for believing the predominant molecular species in the solvent to be Se_8. If one takes a saturated solution of Se in CS_2 and places several drops on a microscope slide, the CS_2 will evaporate in about one minute leaving behind platelets of α-monoclinic selenium with dimensions of the order of 50μ. However, the thermodynamically stable crystalline form at room temperature and atmospheric pressure is the trigonal, which is composed of helical chains. The fact that one observes α-monoclinic crystals precipitated from the CS_2 solution tends to indicate that this is a kinetic process which deposits the molecules in the form in which they exist in the solution (i.e. Se_8). The same experiment with Se dissolved in TCE yields small α crystals. But a

much larger proportion of the selenium is deposited in what appear to be amorphous globs than is the case with CS_2 solutions. This may indicate that in the case of TCE the selenium exists in the solution in other molecular forms besides Se_8. On the assumption that Se_8 is the predomination molecular species, the molar extinction coefficient is indicated on the right of figure 4.

Examining figure 4 one observes the extinction coefficient, ϵ, to increase approximately linearly with increasing photon energy from the onset of significant absorption in the vicinity of 2.7 eV to the vicinity of 3.3 eV for both the CS_2 and the TCE solutions. In the vicinity of 3.3 eV the slope of ϵ steepens for both solutions. Beyond this point the absorption of the CS_2 limits the range of measurement. The TCE data show a peak at 3.8 eV, a valley at 4.0 eV followed by an increase of undetermined extent.

The similarity of the shapes of the CS_2 and TCE curves at lower energies argues in favor of the same molecules in each while the difference in amplitude argues for a concentration difference for this molecule species in the two solutions. One possibility would be for there to be a preponderance of Se_8 molecules in the CS_2 while in the TCE about one half of the selenium is in the form of other molecular species. If a membrane which is permeable to the solvents, but not to Se_8 could be found, measurements of osmotic pressure could determine the molecular fractions.

Comparison of "ϵ" for the case of the solid to the case of the solution (see figures 3 and 4) shows that in the solid the absorption edge has been shifted in energy by about 0.5 eV. However, $d\epsilon/dE$ in

the linear regions of the two curves is approximately the same. This would lead one to believe that the intermolecular interactions in the solid, while not small (certainly stronger than Van der Waal's interactions), do not grossly perturb the density of states or the transition matrix elements.

Summary

The optical absorption of selenium in the α-monoclinic crystal and in solutions of organic solvents has been observed. The absorption edge is 2.25 eV for the former and 2.7 eV for the latter. The intermolecular bonding is stronger than Van der Waal's in this crystal.

PART II

Introduction

We discuss here the processes involved in carriers entering α-monoclinic selenium from a metallic contact and then moving through the bulk. Although Gudden and Pohl, in 1926, noted the existence of both positive and negative current flow and, also, noted the absence of current flow in the absence of illumination, no one has yet called attention to the fact that if carriers are mobile in the lattice and yet no current flows between metallic contacts applied to the material if bias is applied, carriers must be blocked from entering the lattice.(5) In the study reported in the first chapter of this part, the nature of the contacts was probed by observing the variation of current which flowed through the sample under the influence of applied bias as the wavelength of monochromatic light impinging upon the sample was changed. Examination of these results, with contact area and contact material as variable parameters, allows the existence of surface barriers to be demonstrated and allows their energy to be determined.

In the second and third chapters, we discuss the results of experiments in which charges were photo-generated just under one contact and drawn across the bulk under the influence of an applied bias field. From the temporal variation of the integrated current arising from this moving charge, information concerning the mobility can be deduced. By examining the variation of this current as the sign and amplitude of the applied field, temperature, and light intensity are varied, the magnitudes of the electron and hole mobilities, the mechanisms controlling these mobilities, and the mechanism controlling the collection

efficiency for carriers are educed.

CHAPTER I

Surface Barriers

1.1 Sample Preparation

The method of growing the crystals used in these studies was reported earlier.[9] Samples were prepared by lapping α-monoclinic, single crystals to platelets of the desired thickness and then etching the platelets in spectroscopic grade CS_2 in order to remove any surface damage resulting from the lapping. The crystals were oriented prior to lapping so that the large surfaces which received the contacts lay in the (101) plane. Because the α-monoclinic form is thermodynamically unstable at room temperature and pressure - converting to the trigonal form in a period of a few years under these conditions[13] - care was exercised throughout this procedure to avoid heating the crystals above room temperature (20-25°C) in order to avoid thermal damage to the crystal. The resulting platelets were 30 to 100 μ in thickness and had lateral dimensions of few mm.

Metallic contacts were made to the two sides of the platelets. One side, which will be referred to as the back, was placed in contact with a copper substrate. Back contacts were made of gold or gallium while the front contact always consisted of a semitransparent gold dot deposited by vacuum evaporation. A shutter was used in all evaporations in order to minimize exposure of the crystal to the hot filament and thus minimize thermal damage from this source. The gold back contacts were vacuum evaporated and then cemented to the substrate with silver

paste. The gallium back contacts were prepared by first wetting the copper substrate with gallium. In the course of this process enough copper was dissolved in the gallium to depress the melting temperature to below room ambient ($\sim 23^{\circ}C$). The selenium platelet was then pressed into the liquid gallium. This rather unorthodox procedure for fabricating the gallium contact was used because selenium reacts chemically with most metals. The low temperature encountered in the procedure described above restricts the reaction rate to a low enough value that the desired measurements can be made long before detectable reaction occurs.

1.2 Experimental Procedure

As was remarked earlier, this study consisted of a series of experiments in which monochromatic light was directed onto the front of the sample and the current observed as a function of light wavelength. In experiments of this type, one expects essentially no current until the photons can give the electrons in the metal enough energy to go over the barrier into the insulator. Once this barrier threshold is exceeded, one expects the current to increase with increasing photon energy as more and more transitions which enable an electron to go over the barrier become allowed.[14] As photon energies increase, the threshold for directly exciting free carriers in the insulator is exceeded, causing a very rapid increase in current.

Monochromatic light, for these experiments, was provided by passing a chopped light beam through a Spex model 1400-11 double grating monochromator. Second order light, a phenomenon inherent to all grating monochromators, is especially deleterious for these experiments because

of the much greater efficiency of light of shorter wavelength as a generator of free carriers - as noted above. Problems from this source were avoided by utilizing polished crystals of the series CdS_xSe_{1-x} as filters of the beam exiting from the monochromator. The exact composition of the filter crystals depended upon the range of wavelengths desired. If the absorption edge of the filter lay at E_a, then the photon energies used in the experiment would lie in the range 0.5 E_a to E_a. In no case was it possible to detect light emerging from the monochromator on the short wavelength side of E_a.

The light emerging from the monochromator was focussed by means of a front-surfaced, reducing mirror onto the front of the platelet. The light imaged on the sample in a spot which covered the crystal. Bias was applied to the crystal by applying voltage between the copper substrate and a .002" gold wire pressed against the front contact. The photocurrent flowing in this circuit was amplified, synchronously detected, and read from a digital voltmeter. Reversing the polarity of the bias allowed the current from the front and back contacts to be investigated separately. Some measurements were made employing guard rings to assure that the current flow was predominantly through the crystal and not along its surface.

1.3 Results and Discussions

In Figure 5 is plotted the logarithm of the photocurrent versus photon energy for two polarities of bias for a sample which had both front and back contacts of gold, but for which the ratio of the area of the front contact to that of the back contact was about 1:13. The high energy portions of the two curves are quite similar, as would be

expected for bulk free carrier creation in a crystal in which both carrier species are mobile. The energy at which the current begins to increase quite rapidly, 2.3 eV, is in good agreement with the earlier reported value for the optical absorption edge for α-monoclinic selenium.

Below about 1.8 eV, the current is increasing as would be expected from injection over a barrier, but the ratio of the currents for the two polarities is $\sim$ 40:1. Simple considerations of area of contacts accounts for a difference of 13:1. The higher efficiency of the back contact relative to the front is accounted for by recalling that the optical absorption length in gold for the wavelengths of interest is in the range 130 Å to 150 Å and that the range in gold for hot electrons of the energies involved in this experiment is about 350 Å.[15,16] Taking the thickness of the front contact to be about 900 Å, one sees that the electrons are essentially all generated at the front surface of the gold and then relax as they diffuse toward the selenium so that those which reach the selenium surface with enough energy to surmount the barrier are down to about $1/e^2$ of those which initially had enough to do so. On the basis of these considerations the rear contact should be about 10 times as efficient at injecting electrons into the selenium as the front contact. It will be shown later that about 70% of the photons of these energies which enter the selenium are absorbed before reaching the rear contact leaving the rear contact more efficient by a factor of $\sim$ e and bringing the observed values into good agreement with expectation. It should be remarked in passing that the polarities of the bias involved in this experiment argue strongly for the carriers

injected over the barriers being electrons.

The only seeming discrepancy from expectation is the sharp dip that occurs in the electrons coming from the back contact at photon energies between 1.9 eV and 2.1 eV. Prosser's work, however, shows a sharp increase in the optical absorption constant of from $.166 \times 10^{+3} cm^{-1}$ at 1.9 eV to $1.805 \times 10^{3}\ cm^{-1}$ at 2.1 eV.(6) Since this platelet was measured to be about 100 μ thick the percentage of light entering the selenium crystal which reaches the back contact is about 30% at energies < 1.8 eV, 19% at 1.9 eV, 0.18% at 2.0 eV and 1.4×10^{-6}% at 2.1 eV. Since it is clear that this absorption must account for a decrease in photocurrent, the electron which absorbs the photon must make a transition between two localized states (e.g. a bound exciton). As the energy of the photons increases, the energy which separates the absorbing localized states from the conducting states decreases and it becomes increasingly likely that a phonon will supply the energy necessary to allow the electron to become mobile and contribute to the current. At about 2.1 eV, the current from this process dominates the current coming over the barriers for both polarities and continues as the dominant process until the photon energy is increased to the threshold for photogeneration of free carriers.

Turning to Figure 6, one sees the square root of the normalized photocurrent plotted as a function of energy of incident photons for a sample with gold front contact and gallium back contact. This plot is linear over a large range of photon energy. The zero current intercept for the case in which the gold contact was biased negatively is about

1.3 eV, as it was for similar plots of cases in which both contacts were gold. However, in the case in which the gallium is biased negatively, the zero current intercept is 1.05 eV. This clear cut difference of threshold with differing contact materials demonstrates that this is indeed a contact phenomenon.

The sign of the bias indicates that the carriers being injected are electrons. The barriers to the injection of electrons from gallium and gold into Se are 1.05 eV and 1.3 eV, respectively. The electronegativity of gallium is 1.6 and that of gold is 2.4.[17] Thus, the ratio of the change of barrier height to the change of electronegativity is considerably less than one. Earlier authors have associated this condition with surface states in the middle of the zone of forbidden energy arising out of the large overlap of the wavefunctions in covalently bonded crystals.[18] The present results seem to support these views.

CHAPTER II

Transient Measurements

2.1 Experimental Procedure

Samples used in these experiments were prepared as described in the previous section. In all cases, both front and back contacts were of gold. As mentioned previously, the measurement consisted of generating carriers at the front surface with a flash of light and drawing the generated carriers across the crystal with an externally applied bias field. The light flash for these measurements was provided by a

theta pinch discharge lamp (Fischer Nanolite) with a half width of about 10 nanoseconds. This light was focussed onto the sample by a front surfaced mirror. A #5-60 Corning glass filter limited the light reaching the crystal to those wavelengths which are strongly absorbed by α-monoclinic selenium. (The filter passes light in the wavelength range 0.33 μ to 0.52 μ. The absorption length in α-monoclinic selenium for light of these wavelengths ranges from 0.2 μ to 0.02 μ.) The intensity of light reaching the sample could be controlled by neutral density filters of metal screen (in some cases mechanically supported by ultrasil fused silica) placed in the light beam. The density of the neutral density filters was calibrated with a Cary model 14 spectrophotometer.

The sample was contained in an electrostatically shielded box which was electrically integral with the amplifier. This shielding was to isolate the measuring circuit from the r.f. pulse produced by the plasma arc coincidentally with the light. Provision was made for hermetically sealing this box after putting dessicant in it in order to avoid condensation of water on the sample while making low temperature measurements. The box contained a copper block whose temperature could be controlled by passing gas through a hole drilled through it. Plastic tubing connected the hole through the block to copper tubes which pierced the side of the box. The copper substrate, on which the selenium crystal was mounted, was held firmly pressed against the copper block. The temperature of this assembly was monitored by a thermocouple affixed in intimate thermal (but not electrical) contact with the copper block.

The external bias was applied between a .002" diameter gold wire pressed against the front electrode and the copper block. The current, which arose from the optically generated carriers crossing the crystal, was integrated by a passive RC integrator with a time constant of about 800 μ sec (very much greater than any measured transit time), amplified by a Keithley model 105 pulse amplifier, and displayed on a high speed oscilloscope. The data were photographically recorded from the oscilloscope screen. Since the carriers were generated in a distance very much less than the thickness of a platelet (typically ~ 40 μ), the applied field pushed carriers of one sign almost instantaneously into the front contact while drifting carriers of the other sign across the platelet to the back contact. Because of the extremely small ratio of generation length to sample thickness (~ 1/500), the current arising from the charges going to the front contact contributed a negligible amount to the integrated current which can, therefore, be considered as arising from a unipolar sheet of charge drifting across the crystal as long as the generation time (i.e. duration of the light flash) is much less than the time for the carriers to drift across the platelets - a condition which was met in all of these experiments. The sign of the carriers composing the charge sheet could, of course, be changed by changing the polarity of the applied bias. In order to insure that the bias field was not distorted by trapped charge, the sample was shorted and illuminated with ten light pulses before each measurement.

2.2 Transit Time

The simplest model for these experiments treats a rigid charge sheet which drifts across the sample at a uniform rate. In this case

the current is constant and the integrated current increases linearly with time until the charge reaches the back contact, beyond which point the current drops to zero and the integral remains constant. Trapping, diffusion, and space charge effects can all affect this simple model, as shall be discussed. It, nevertheless, is a good approximation in many instances and serves as a convenient starting place for introducing modifications. In this model, one defines a transit time, τ_t, as the period from the beginning of the increase in integrated current (i.e. the time of the charge generation) to the end of the increase in integrated current (i.e. when the carriers reach the back contact). Utilizing this definition and the definition of mobility, one arrives at

$$\mu = \frac{1}{\tau_t} \frac{d}{E} \tag{1}$$

where μ is the mobility, d is crystal thickness and E is the field applied across the sample. In figure 7 is shown a typical oscillograph of integrated current, $Q(t)$, as a function of time. The charge (i.e. integrated current) can be seen to increase reasonably linearly with time. There is some rounding at the corner and a slow tail. If the experiment is performed without the Corning filter, the magnitude of the slow tail is greatly increased. The transit time is defined for this experiment as the time between the onset of the current and the time at which the extrapolation of the linear portion of the charge increase reaches the level of the total charge transferred.

One factor which affects the simple model previously introduced is trapping. Trapping has been treated by a number of authors.[19]

Only two limiting cases will be discussed here: the case of "deep" trapping in which the trap release time is very much longer than the transit time, τ_t, and the case in which the trap release time is much less than the transit time.

For deep trapping, the probability of a carrier being trapped between t and t+Δt is just $p(t) = BN_t(1-f)$ where B is the probability that one empty trap will trap in one second a single free carrier which has been released in a unit volume of material, N_t is the trap density, and f is the probability that the trap is occupied. If one assumes that f is constant and that the release time is infinite, the number of free carriers at time, t, ($t \ll \tau_t$, the transit time) is given by $n(t) = Q_o \exp(-BN_t(1-f))$ where Q_o is the initial number of carriers. Under these conditions one can define a trapping time $\tau_{tr} \equiv 1/BN_t(1-f)$. Since the current, i(t), is given by $i(t) = \mu En(t)/d$ where, as before, d is the crystal thickness, the integrated current

$$Q(t) = \int_o^t \mu En(t')dt' = \begin{cases} \frac{\mu EQ_o\tau_{tr}}{d}\left[1-\exp(-t/\tau_{tr})\right] & t \leq \tau_t \qquad (2a) \\ \frac{\tau_{tr}\mu EQ_o}{d}\left[1-\exp(-\tau_t/\tau_{tr})\right] & t > \tau_t \qquad (2b) \end{cases}$$

The latter equation is, of course, just the Hecht result.[20]

In figure 8, eq. (2) is plotted for various ratios of τ_{tr}/τ_t. Note that for $\tau_{tr} \gg \tau_t$ the pulse shape is essentially undisturbed and the measured transit time, as defined earlier, would agree with the true (i.e. untrapped) transit time, while for $\tau_{tr} \ll \tau_r$ the pulse shape is

considerably distorted and the measured transit time would approximate the trapping time, not the true transit time. Measurement allows one to determine whether the transit time is greater or less than the trapping time for deep traps. Equation (1) shows that in the case $\tau_{tr} > \tau_t$, $1/\tau_t$ varies linearly as a function of E. However, as noted above, the measured $(1/\tau_t)$ is independent of E for the case $\tau_{tr} \ll \tau_t$ and follows a non-linear relationship as τ_{tr} nears τ_t. Figure 9 shows a plot of $(1/\tau_t)$ vs. E for a typical sample biased such that holes were the carriers traversing the crystal. This linear behavior was observed for both polarities on all cases in which space charge did not play a part. Thus, one can conclude that deep trapping played little part in the measurements reported here.

The limit in which the trap release time, τ_R, is much less than the transit time is in some ways simpler than the opposite limit. In the short release time limit, one can distinguish two cases: either the trapping time is very much greater than the release time or the trapping time is near or less than the release time. If the trapping time is much greater than the release time, the carriers are essentially always free and the measured mobility is equal to the microscopic mobility. If the trapping time is near or less than the release time, Tefft has shown that one measures an effective mobility, μ_{eff}, given by the equation

$$\mu_{eff} = \mu_o \left(\frac{\tau_{tr}}{\tau_{tr} + \tau_R} \right) \tag{3}$$

where μ_o is the microscopic mobility.[19] He also shows that the shape

of Q(t) as displayed on an oscilloscope is essentially unchanged from the case of no trapping. It is clear from eq. 3 that if $\tau_{tr} \ll \tau_R$, $\mu_{eff} \cong \mu_o \tau_{tr} \frac{1}{\tau_R}$. Since $\frac{1}{\tau_R} \alpha \exp(-E_t/kT)$ as long as the traps are several kT above the Fermi level, where E_t is the trap activation energy (i.e. the energy difference of the trap and the conducting states)

$$\mu_{eff} \alpha \mu_o \exp(-E_t/kT). \tag{4}$$

In this case, the measured mobility varies exponentially with 1/T, but the microscopic mobility cannot be determined unless the sample can be taken to a high enough temperature that τ_{tr} becomes comparable with τ_R.

Another factor complicating the simple model presented so far is space charge, the effect upon one carrier of the fields from all the other carriers. This problem has been treated in detail by S. Z. Weisz et al for the case of carriers generated by a short pulse of light.(21) As long as the carriers which are generated at the front surface must either all begin to drift across the sample or recombine in a time short with respect to the transit time, no virtual cathode (i.e. a reservoir of charge which makes E = o) can form. Simple integration of Poisson's equation then shows that the maximum amount of charge which can be drawn across the platelet is CV where C is the parallel plate capacitance of the sample and V the applied voltage. It will be shown later that the condition of having no virtual cathode must hold for these experiments. In figure 10 is shown the result of a graphical integration of the curves presented by Weisz et al. for current as a function of time. In this figure, the integrated current,

or charge, $Q(t)$, is normalized by dividing it by the total charge generated, Q_o, and plotted versus time. Note that the transit time, as it has been defined above for use with experimental data, increases about 20% as Q_o increases from 1/10 CV to CV, and that most of the increase in τ_t occurs as Q_o increases from 1/2 CV to CV.

Turning from theory to experiment, figure 11 shows the total charge transferred across the crystal, Q_T, and τ_t plotted as a function of light intensity. Note that Q_T increases to CV - and then exceeds it by 40%, a difference far greater than any experimental error. Two possible explanations for this behavior exist. This first is that a sufficiently large charge reservoir is established to create a virtual cathode which persists for an appreciable fraction of the transit time. It will be shown in a later section that in the experiments discussed here, any reservoir must collapse in a time very much less than the transit time. A second possibility is seen by noting that extrapolation of the low intensity portion of the Q_T curve suggests that a surface density of carriers of between $10^{16}/cm^3$ and $10^{17}/cm^3$ is created by the light flash. This would cause the surface sheet resistance of the selenium crystal to be in the vicinity of a few hundred ohms/□ which is within an order of magnitude of that of the evaporated gold contact. Since the evaporated contact covered only about 1/10 of the surface, it is possible that the surface conductivity was modulated by the light flash to such an extent that the effective area of the contact increased enough that Q_T is equal to an "effective" CV. This would explain the large increase in transit time for the case with Q_T > CV

because after the initial charge injection from the modulated surface the field lines would change rather drastically as the surface resistance rose. Note that the transit time increases approximately the 20% previously predicted as Q_T increases from ~ 0.1 CV to CV. Note also that as Q_T increases from ~ 0.1 CV to about 0.5 CV, τ_t increases only a small amount, in line with previous predictions. In order to avoid the complications introduced by space charge effects, the data to be discussed in the remainder of the paper were taken with a neutral density filter of density 1.295 D.U. in the light beam which reduced Q_T to a maximum value of less than 20% CV.

In the course of these measurements, the relative dielectric constant, K, was measured over the frequency range, 100 kHz to 100 MHz and found to be $9.2 \pm .6$. That this value is higher than that of Kyropoulos is not surprising since Gudden and Pohl comment that they were prevented from making optical absorption measurements by the multiplicity of voids in Kyropoulos' crystals.[4,5]

The final consideration is the effect of diffusion upon the carriers as they drift across the bulk of the sample. Since the forces of drift and diffusion are independent in this case, one can solve the equations separately and then combine the solutions. The solution to the diffusion equation for the initial condition of a delta function is

$$n(x,t) = Q_o \frac{q}{4\pi kTt\mu} \exp\left(- qx^2/4tkT\mu\right) \qquad (5)$$

where q is the magnitude of the charge on the electron. Evaluating eq. 5 at the transit time yields

$$n(x) = Q_o \frac{qE}{4\pi kTd} \exp(-qEx^2/4kTd) \qquad (6)$$

For values typical for the experiments discussed here, the distribution given by (6) has a width equal to about 10% of d. Thus, diffusion has a small effect upon the transit time of the carriers crossing the crystal, but will cause the corner of the Q(t) vs. t curve to be rounded over the last 10% of the transit time.

From the previous discussion, it can be seen that in these experiments the true transit time was measured. It is clear from eq. (1) that in this case the slope of a plot of $1/\tau_t$ versus E yields the mobility. The mobility was determined in this way for carriers of both signs, as a function of temperature. In figure 12 is plotted the logarithm of the hole mobility versus inverse temperature for one sample. The circles, representing data taken as the temperature was being increased toward the maximum value employed, fall essentially on a straight line, implying a trap limited mobility. The slope of this line yields a trap activation energy of .24 eV. Measurements on a number of samples consistently give a hole trap activation energy of .23 ± .01 eV. The squares in figure 12 represent data taken after the sample was heated to the highest temperature utilized in these measurements, 50°C. Note that they are of the same slope as the data taken earlier, but have lower values than the earlier data. This implies that traps with activation energy equal to that of the traps previously present have been thermally introduced into the sample, suggesting a common origin. One strongly suspects, but cannot prove, that these hole traps are caused by lattice disorder, probably Se_8

rings which have broken open.

Figure 13 shows electron mobility plotted as a function of $T^{-3/2}$ for the same sample on which the data shown in figure 12 were taken. The squares in this case again represent data taken after heating the sample. It should be noted that within experimental error these have the same values as their earlier counterparts. The linear form of this graph is in agreement with Spear, who also found the electron mobility to vary as $T^{-3/2}$ and attributed this result to lattice scattering.(8) The room temperature electron mobility was found to vary from 1.5 cm^2/V sec to 3.6 cm^2/V sec in a number of measurements on samples taken from a number of batches of crystals grown at different times under slightly different conditions.

CHAPTER III

Collection Efficiency

As one can readily observe from figure 14, all of the carriers generated are not always collected at the rear contact; for Q_T varies with bias field, E. (The scatter in data at a given field is caused by variation from pulse to pulse in the light intensity striking the sample.) The ratio of carriers generated to those collected at the back contact

$$\frac{Q_T}{Q_o} \equiv \eta$$

where η is defined as the collection efficiency. Various mechanisms can be proposed to explain the variation of η with E: trapping without

release in the bulk, recombination in the region of generation, deep trapping near the surface, field-controlled photogeneration, and diffusion of the carrier to the metal contact. It will be shown that only the latter process fits all of the available data for the case under discussion here and an analytic expression for η will be calculated.

It was argued in the previous chapter that deep trapping without release was not an appropriate consideration for this case because of the linearity displayed in the $1/\tau_t$ vs. E plot of figure 9. Figure 15 shows further evidence on this point. The solid line in the figure is a tracing of an oscillograph of $Q(t)$ vs. time for the sample of figure 14 biased at 1,160 V/cm. The dashed line in this figure represents what this curve would look like for this case if η were dominated by deep trapping.

To discuss recombination in the region of generation, a model is needed. Since it was shown in the previous section that holes spend most of their time in shallow traps while electrons are not trapped in any detectable amount, the model used will be one in which all of the holes are in shallow traps which act as recombination centers when so occupied. The question becomes whether the time for an electron to cross the recombination region is greater or less than the recombination time under these conditions.

The probability of an electron recombining in unit time,

$$P_r(t) = \upsilon_{th} N_t f' \sigma$$

where υ_{th} is the thermal velocity, σ is the capture cross section of the trap for electrons, N_t is the trap density, and f' is the occupation factor which gives the fraction of the traps occupied by a hole.[22]

$$N_t f' = Q_o \alpha / A$$

where α is the absorption constant and A is the area of the contact. Since both the transmission of the filter and the spectral intensity of the source peak in the vicinity of 4200 Å, α will be taken to be $2 \times 10^5 cm^{-1}$, the value at 4200 Å.[23] Assuming that $\upsilon_{th} = 10^7$ cm/sec, that $\sigma = 10^{-15} cm^2$, the cross sectional area of an Se_8 molecule, and that $Q_o \cong Q_{Imax}$, one finds that that recombination time is

$$\frac{1}{P_r} \cong 200 \text{ nsec}$$

while the time for an electron to cross the absorption region at a field of 1000 V/cm (a value at which half of the carriers must recombine if recombination is to be a tenable mechanism for the η variation) is about 1 nsec. Thus, the recombination rate is too small by about two orders of magnitude to explain the observed effect.

One could easily imagine that deposition of the contact caused considerable damage to the crystal near the surface, resulting in a very large trap density extending a distance, ℓ, into the crystal. If $\ell \ll d$, then one cannot rule it out by the arguments made to eliminate the Hecht process. Arguments analogous to the Hecht analysis show that

$$Q_t = Q_o e^{-\ell \tau_{tr}/\mu E}$$

$$\exp\left(-\ell/\tau_{tr}\mu E\right)$$

where τ_{tr} is the trapping time. Values of Q_o, ℓ, and τ_{tr} could certainly be chosen to fit the data of figure 14, but, as figure 16 shows, Q_t is quite close to being the same for holes and electrons. It would indeed be fortuitous if $\mu\tau_{tr}$ were the same for holes and electrons in the hypothetical damaged layer. Yet Q_t depends <u>exponentially</u> upon $\mu\tau_{tr}$. The improbability of the coincidence of $\mu\tau_{tr}$ for electrons and holes makes this explanation for the variation of η with E rather untenable.

Tabak and Warter have recently proposed that in some materials photons may excite carriers to non-conducting excited states from which they must be ejected into conducting states.[24] They further suggested that this may occur in a manner similar to the Poole-Frenkel effect, thus giving rise to a field dependent η. To be precise they find

$$\eta = \left[1 + \frac{1}{\tau_r \nu} \exp\left(\frac{\xi_t - e\beta E^{1/2}}{kT}\right)\right]^{-1}$$

where τ_r is the rate of nonphotoconductive decay of the exciton, ν is the attempt-to-escape frequency, ξ_t is the binding energy of the exciton, e is the charge on an electron, and $\beta = \left(\frac{e}{\pi\epsilon}\right)^{1/2}$ where ϵ is the dielectric constant. The temperature dependence is strongest at low fields where the numerator of the exponent is largest. Figure 17 shows data of Q_T as a function of temperature at a field of 1,160 V/cm. The solid line represents a least-squares fit to the data. The least-squares fit <u>decreases</u> about 10% as the temperature increases 50°C while the Poole-Frenkel effect requires η to increase <u>exponentially</u> with T.

The last model to be considered is based upon diffusion of carriers to the front contact. If a carrier diffuses from the selenium crystal into the front contact, it may either relax into the Fermi sea or diffuse back into the selenium. The time for a hot electron to relax into the Fermi sea in gold is the range of the hot electron divided by the Fermi velocity or about 10^{-14} second. The carriers which relax into the Fermi sea become uniformly distributed throughout the contact in the dielectric relaxation time $\tau_D = \frac{\epsilon}{\sigma}$, which for gold is about 10^{-19} seconds.[25] These times are so low that the concentration of carriers at the gold selenium interface will be taken to be zero. As carriers diffuse to this interface, they relax into the metal and are lost from the charge cloud. The applied field competes with this process (for carriers of one sign) by drifting the carriers away from the contact. In this calculation only the carriers of the sign being drifted across the sample are considered; it is assumed that carriers of the other sign are immediately swept into the front contact and can, hence, be neglected. It is also assumed that the charge density is low enough that space charge effects are small and that the field can, therefore, be taken as independent of position, as has been previously shown to be true for these measurements.

One begins with the continuity equation

$$\frac{\partial n}{\partial t} = D\frac{\partial^2 n}{\partial x^2} - \mu E\frac{\partial n}{\partial x}$$

where n is the carrier density, E is the dielectric field, and D is the diffusion constant. Since the Einstein relation is $D = \mu\frac{kT}{q}$, one

can see immediately that the relative magnitude of the processes of drift and diffusion are independent of mobility and that carriers of both polarities should behave similarly.[26] The detailed solution of this equation with the boundary conditions $n(o,t) = n(d,t) = o$ and the initial condition

$$n(x,o) = \begin{cases} N_o e^{-\alpha x} & x > o \\ o & x \leq o \end{cases}$$

where α is the optical absorption constant is carried out in appendix II. It is shown there that either the carriers diffuse to the surface and relax in a time short with respect to the transit time or they drift away and cross the crystal. The collection efficiency,

$$\eta = \frac{Q_T}{Q_o} = \frac{E/E_f}{1+E/E_f}$$

where $E_f \equiv \frac{\alpha kT}{q}$. This function is plotted as the heavy line in figure 14 with Q_o adjusted to make the curve match the data at the field 6,970V/cm. As can be seen the agreement of theory to experiment is really quite acceptable. The theory also predicts that Q_T should decrease about 10% between 0^oC and 50^o for the case exhibited in figure 16, in fortuitously good agreement with experiment. As already noted, η is expected to be the same for carriers of both polarities, in agreement with the results of figure 16.

SUMMARY

This work has shown that metals in intimate contact with α-monoclinic selenium form barriers to the injection of electrons and holes into the selenium. The electron barriers are 1.05 eV in the case of gallium and 1.3 eV in the case of gold; demonstrating again the hazards of attempting to characterize insulators by means of resistance measurements.

A large increase in the photocurrent at 2.3 eV was taken to indicate the onset of the creation of free electrons and holes in good agreement with our measurements of the optical absorption edge. It was also concluded that optical absorption at wavelengths longer than this edge may be attributed to the creation of localized excitations.

Transient measurements have shown the room temperature electron mobility varies from 1.6cm^2/V-sec to 3.6 cm^2/V-sec according to details of the conditions of crystal growth. The temperature dependence of the electron mobility was found to be $T^{-3/2}$ in agreement with Spear who attributed the dependence to lattice scattering.(8) The hole mobility was found to be controlled by shallow traps with an effective depth of 0.23 eV ± .01 eV. It has been shown here that these traps can be thermally generated by heating to the vicinity of 50°C suggesting that these traps arise from lattice imperfections, such as broken Se_8 rings. A typical room temperature hole mobility was found to be 0.2 cm^2/V-sec, but this, of course, varied noticeably according to the trap density.

The variation of collection efficiency, η, (i.e. the ratio of the number of carriers collected at the back contact to the number created

at the front contact) with field is discussed and it is shown that this most probably results from the interplay between diffusion, which carries the carriers into the front contact where they relax, and electric field, which drifts the carriers toward the rear contact. An analytic expression for η is derived.

OVERVIEW

In the course of this thesis, the author has become aware of two general reasons for studying α-monoclinic selenium. The first is that this material presents an intermediate case between the extremes of covalent crystals (e.g. silicon and germanium) and molecular crystals (e.g. benzene and anthracene). The second is that α-monoclinic selenium provides an extraordinarily good opportunity to study transport phenomena.

To expand on the first point, the reader is reminded that the Se_8 molecules, which make up the α-monoclinic crystal, are also believed to exist in solutions with organic solvents which can be sufficiently dilute that interaction between the Se_8 molecules is negligible. Furthermore, trigonal selenium is composed of long chains in which the interatomic distances and bond angles are virtually identical to those in the Se_8 rings, while the density is about 10% higher than that of the α-monoclinic form because of decreased intermolecular spacing.[29] Thus, one has the opportunity to observe what effect decreasing the intermolecular spacing has upon the physical properties of selenium. In solution, where we consider only intramolecular forces, the optical absorption edge is 2.7 eV. In the α-monoclinic crystal, the most important bonding is surely intramolecular since the intramolecular bond is 1.2 Å shorter than the nearest intermolecular distance.[7] Nevertheless, the optical absorption edge shifts to 2.3 eV. For the case of trigonal selenium, the energy of the optical absorption edge is reduced to 1.8 eV.[29] It seems highly probable that these decreases

in the energy of the optical absorption edge are a result of increased overlap of wavefunctions of neighboring molecules. One must conclude from this that calculations such as those of Olechna and Knox and of Reitz which completely neglect intermolecular forces are seriously in error.[30,31] Von Hippel and Burbank have reached similar conclusions on different grounds.[32,7]

One can see that selenium does form an intermediate case between the covalently bonded materials such as silicon and germanium where a collective description of the whole crystal seems appropriate and materials such as crystalline benzene and anthracene where the optical excitations seem to be essentially unchanged from those exhibited by the molecules in the gaseous state.[33]

This "intermediate" quality may be reflected in the mobilities. "Perfect" covalently bonded crystals typically have room temperature mobilities of a few thousand. A typical mobility for an organic molecular crystal (where molecule to molecule hopping may be an appropriate model for charge transport) is 10^{-3}.[34] The "intrinsic" carrier mobilities in α-selenium seem to be of order of magnitude one.

In addition to the interest in α-selenium as an intermediate between covalent crystals (one huge molecule) and molecular crystals (many small molecules hung together), the crystal seems to be an ideal one in which to study various charge transport mechanisms. The linearity of the $1/\tau$ vs. E curves at fields near 1000 V/cm and the fact that approximately equal collection efficiencies are seen for both electrons and holes at low fields ($\sim$ 1000 V/cm) both imply a net ionized impurity

density of less than $10^{12}/cm^3$; perhaps this is because impurities fit into Se_8 rings so poorly that the impurities tend to go into interstitial positions between the rings where they are essentially electrically inactive. Another facet of selenium is that the carrier lifetime is extremely long (a fact of considerable importance technologically in the xerographic process) and the rate for deep trapping extremely low for carriers of both polarities. All these properties, when taken together, make this material almost ideal for transient analysis because the experiments are so "clean".

It seems to the author that only a beginning has been made on the possibilities inherent in this material. If large crystals could be obtained, optical reflectance measurements could be made which when analyzed with the Kronig-Kramers formalism would yield the complex index of refraction over a wide range. A combination of this information with the work of Saffren[35] should allow identification of the transitions which give rise to the absorption. Preliminary investigations have shown that the optical absorption edge of α-monoclinic selenium shifts rather drastically with temperature. Combination of measurements of the temperature dependence of the optical absorption and the temperature dependence of the spacings in the α-monoclinic crystals might allow estimates to be made of the relative contributions of various forces contributing to the absorption spectra.

It is also felt that the advantages α-selenium offers for transport measurements have not been exploited to their fullest extent. For example, it is to be expected that experiment on thicker samples than were generally used in this work would yield useful information concerning deep trapping processes.

APPENDIX I

In attempting to unravel the transmission data, one is faced with solving the problem of light passing from one medium through two dissimilar media, reemerging into a medium of the same index as the original medium. This problem may be solved in a straightforward, if tedious, manner by requiring the solution of the wave equation and its derivative to match at all three boundaries. Under the simplifying assumption of no absorption in the second layer (e.g. the quartz substrate in our case) the solution reduces to

$$T = 16/\left[G_1 + G_2 \cos\left(4\pi\eta_2 d/\lambda\right) + G_3 \sin\left(4\pi\eta_2 d/\lambda\right)\right] \qquad (1)$$

where T is the ratio of transmitted to incident power, d is the thickness of the second layer, η_2 is the index of refraction of the second layer, and λ is the free space wavelength of the incident light.

$$G_1 = \left(A_1^2 - A_2^2 - A_3^2 - A_4^2 - A_5^2 + A_6^2\right) \cos\left(4\pi n\, a/\lambda\right)$$

$$2(A_1A_5 + A_3A_6) \sin\left(4\pi na/\lambda\right) + 2(A_1A_4 + A_2A_6) \sinh\left(4\pi ka/\lambda\right)$$

$$\left(A_1^2 + A_2^2 + A_3^2 + A_4^2 + A_5^2 + A_6^2\right) \cosh\left(4\pi ka/\lambda\right) \qquad (2)$$

$$G_2 = \left(A_1^2 + A_2^2 + A_3^2 - A_4^2 - A_5^2 - A_6^2\right) \cos\left(4\pi na/\lambda\right)$$

$$+ 2\,(A_1A_5 - A_3A_6) \sin\left(4\pi na/\lambda\right) + 2\,(A_1A_4 - A_2A_6) \sinh\left(4\pi ka/\lambda\right)$$

$$+ \left(A_1^2 - A_2^2 - A_3^2 + A_4^2 + A_5^2 - A_6^2\right) \cosh\,(4\pi ka/\lambda)$$

$$G_3 = 2\,(A_2A_5 - A_3A_4)\cos\,(4\pi na/\lambda) + 2\,(A_4A_6 - A_1A_2)\sin\,(4\pi na/\lambda)$$

$$+ 2(A_3A_4 - A_2A_5)\cosh\,(4\pi ka/\lambda) + 2\,(A_1A_3 - A_5A_6)\sinh\,(4\pi ka/\lambda)$$

where n and k are respectively the real and imaginary parts of the index of refraction of the first (e.g. selenium) layer, "a" is the thickness of this layer and

$$A_1 = 2$$

$$A_2 = n\left(\eta_2^2 + n^2 + k^2\right)/\eta_2\,(n^2 + k^2)$$

$$A_3 = k\left(n^2 + k^2 - \eta_2^2\right)/\eta_2(n^2 + k^2)$$

$$A_4 = n\left(n^2 + k^2 + \eta_0^2\right)/\eta_0(n^2 + k^2)$$

$$A_5 = k\left(n^2 + k^2 - \eta_0^2\right)/\eta_0(n^2 + k^2)$$

$$A_6 = \left(\eta_2^2 + \eta_0^2\right)/\eta_0\eta_2$$

and η_0 is the index of the initial surrounding media. After considerable work one can show this to be a special case of a general relation derived by Koller.[12]

The question arises of how to handle the sinusoidal terms of argument $4\pi nd/\lambda$. Since the monochrometer has a bandpass of about 10 Å in the configuration in which it was used it seems clear that one should average over the bandpass. Defining $\Delta\lambda$ to be the bandpass and λ_o to be the nominal wavelength one obtains

$$T \cong 16/G_1\left[1 + \left(\frac{G_2^2 + G_3^2}{G_1^2}\right)^{1/2} \cos\left(4\pi\eta_0 d\Delta\lambda/\lambda_0^2 + \theta\right)\right] \qquad (4)$$

where θ is a quantity which doesn't vary during the averaging. Then $\langle T\rangle = \int T d(\Delta\lambda)/\int d(\Delta\lambda)$, but since the argument of the cos goes through many cycles ($\sim$10) as $\Delta\lambda$ ranges over 10 Å

$$\langle T\rangle \cong \frac{N\displaystyle\int_0^{2\pi} \frac{16 d\varphi}{G_1\left[1 + \left(\frac{G_2^2 + G_3^2}{G_1^2}\right)^{1/2} \cos\varphi\right]}}{N\displaystyle\int_0^{2\pi} d\varphi}$$

because the integral over a partial cycle is small with respect to the integral over many cycles. Therefore,

$$\langle T\rangle \cong \frac{16}{G_1\left[1 - \left(\frac{G_2^2 + G_3^2}{G_1^2}\right)\right]^{1/2}} \qquad (5)$$

It might be asked why the cosφ term of equation (4) doesn't average to zero. One way of seeing this is to write

$$\frac{d\varphi}{1 + a\cos\varphi} = d\varphi(1 - a\cos\varphi + a^2\cos^2\varphi + \ldots)$$

and then note that while the first order term does average to zero over a cycle as expected, the second order term is always positive. The effect of the correction term,

$$\frac{G_2^2 + G_3^2}{G_1^2} \quad ,$$

is of the order of .2% to 4% for cases that might be encountered in practice, values that are small enough to justify the approximation made, but large enough to affect the values calculated for n and k.

APPENDIX II

The problem to be solved is that of the behavior of an exponential initial distribution of carriers under the influence of drift and diffusion in the vicinity of a collecting contact. Formally one writes the continuity equation,

$$\frac{\partial n}{\partial t} = D\frac{\partial^2 n}{\partial x^2} - \mu E\frac{\partial n}{\partial x} \tag{1a}$$

the initial condition

$$n(x,o) = \begin{cases} N_o e^{-\alpha x} & X > o \\ \\ o & X \leq o \end{cases} \tag{1b}$$

and the boundary conditions

$$n(o,t) = n(d,t) = o \quad \forall t \tag{1c}$$

where, D is the diffusion constant, n is the number of carriers, μ is the mobility, E is the electric field, α is the optical absorption constant, N_o is the total number of carriers generated at the surface and d is the thickness of the crystal.

Separating variables, solving the equation, and applying the boundary conditions yields

$$n(x,t) = \sum_{m=1}^{\infty} A_m \exp\left[-\left(\frac{n\pi}{d}\right)^2 - \frac{F^2}{4D}t + \frac{Fx}{2D}\right] \sin\frac{m\pi x}{d} \qquad (2)$$

where $F \equiv \mu E$.

Using the initial condition to evaluate A_m, one obtains

$$n(x,t) = \frac{2N_o}{d} \exp\left(-\frac{F^2}{4D}t + \frac{Fx}{2D}\right) \cdot$$

$$\sum_{m=1}^{\infty} \frac{(m\pi/d)\exp\left[-\left(\frac{m\pi}{d}\right)^2 Dt\right]\left\{1 - (-1)^m \exp\left[-\left(\alpha + \frac{F}{2D}\right)d\right]\right\}}{\left(\alpha + \frac{F}{2D}\right)^2 + \left(\frac{m\pi}{d}\right)^2} \sin\frac{m\pi x}{d} \qquad (3)$$

Now if d is very large w.r.t. α, we can let $d \to \infty$ in such a way that $\frac{\ell\pi}{d} \to w$ and obtain

$$n(x,t) = \frac{N_o}{2} \exp\left(-\frac{F^2}{4D}t + \frac{Fx}{2D}\right) \int_0^{\infty} \frac{we^{-w^2 Dt} \sin wx \, dw}{\left(\alpha + \frac{F}{2D}\right)^2 + w^2} \qquad (4)$$

Evaluation of the integral produces [25]

$$n(x,t) = \left\{ \frac{N_o}{2} \exp\left[- \frac{F^2}{4D} t + \frac{Fx}{2D} + \left(\alpha + \frac{F}{2D}\right)^2 Dt \right] \right\} \cdot$$

$$\left\{ \exp\left[-\left(\alpha + \frac{F}{2D}\right) x \right] \operatorname{Erfc}\left[\sqrt{Dt}\left(\alpha + \frac{F}{2D}\right) - \frac{1}{2} \frac{x}{\sqrt{Dt}} \right] - \right.$$

$$\left. \exp\left[\left(\alpha + \frac{F}{2D}\right) x \right] \operatorname{Erfc}\left[\sqrt{Dt}\left(\alpha + \frac{F}{2D}\right) + \frac{x}{2\sqrt{Dt}} \right] \right\} \tag{5}$$

However, equation 5 isn't very useful because what is really desired is the current flow out through the contact at x = o. This current is given by

$$i(t)\Big|_{x = o} = Fn(o,t) - D \left.\frac{\partial n(x,t)}{\partial x}\right|_{x = o} \tag{6}$$

The result of substituting eq. (4) into eq. (6) is

$$i(t)\Big|_{x = o} = \frac{-2N_o D}{\pi} \exp\left[- \frac{F^2}{4D} t \right] \int_o^\infty \frac{w^2 \exp\left[-w^2 Dt \right]}{\left(\alpha + \frac{F}{2D}\right)^2 + w^2} dw \tag{7}$$

The charge lost by time, t, as a result of the current of eq. (7),

$$Q_L(t) = \int i(t')dt' = \frac{-2N_o}{\pi} \left\{ \int_o^\infty \frac{w^2 dw}{\left[w^2 + \left(\alpha + \frac{F}{2D}\right)^2 \right]\left[w^2 + \left(\frac{F}{2D}\right)^2 \right]} \right.$$

$$\left. - \exp\left[- \frac{F^2}{4D} t \right] \int_o^\infty \frac{w^2 \exp\left[-w^2 Dt \right] dw}{\left[w^2 + \left(\alpha + \frac{F}{2D}\right)^2 \right]\left[w^2 + \left(\frac{F}{2D}\right)^2 \right]} \right\} \tag{8}$$

The time dependence is obviously segregated into the second term. Evaluation of the term before the integral places an upper bound on the relaxation time, $\tau_r = \frac{4D}{F^2}$. The ratio of the relaxation time to the transit time

$$\frac{\tau_r}{\tau_t} = \frac{4D}{Fd} = \frac{4kT/q}{V}$$

where V is the voltage across the sample, k is Boltzmann's constant and the Einstein relation has been used to evaluate D.[24] The smallest bias voltage ever employed in these measurements was 5 volts so that

$$\frac{\tau_r}{\tau_t} \leq .02$$

justifying an earlier assertion. Since the second term of eq. (8) drops so rapidly with time (being always less than 1/100 of the first term after $0.1\ \tau_r$), one can say that essentially all of the charge which will be collected at x = o is collected in the first small part of the transit time and approximate the lost charge, $Q_L(t)$, with a constant,

$$Q_L = \frac{2N_o}{\pi} \int \frac{w^2 dw}{\left[w^2 + \left(\alpha + \frac{F}{2D}\right)^2\right]\left[w^2 + \left(\frac{F}{2D}\right)^2\right]} \qquad (9)$$

the first term of equation 8. By evaluating the residues of the poles of the integrand of eq. (9), one finds

$$Q_L = \frac{N_o}{\alpha} \frac{1}{1 + \frac{E}{E_F}} \tag{10}$$

where $E_F \equiv \frac{\alpha kT}{q}$ is an effective "diffusion field." Finally the charge transferred across the crystal is given by

$$Q_T = \frac{n_o}{\alpha} \frac{E/E_F}{1 + E/E_F} \tag{11}$$

REFERENCES

1. Mitscherlich, Berl. Akad. Monatber, 409 (1855).
2. E. Muthmann, Z. Kristallogr. 17, 336 (1890).
3. Saunders, J. Phys. Chem. 4, 423 (1900).
4. S. Kyropoulos, Z. Phys. 40, 618 (1927).
5. B. Gudden and R. Pohl, Z. Phys. 35, 18 (1926).
6. V. Prosser, Cs. Cas. Fys. 10, 35 (1960).
7. Robinson D. Burbank, Acta. Cryst. 4, 140 (1951).
8. W. E. Spear, J. Phys. Chem. Solids 21, 110 (1961).
9. S. Iizima et al., to be published in Proc. 1st Intl. Symp. Physics of Se and Te.
10. J. E. Fergusson et al., J. Inorg. Nucl. Chem. 24, 157 (1962).
11. G. G. MacFarlane et al., Phys. Rev. 108, 1377 (1957).
12. K. Koller, Zs. f. Phys. 110, 45 (1938).
13. R. E. Marsh, private communication.
14. Richard Williams and Richard H. Bube, J. Appl. Phys. 31, 968 (1960).
15. American Institute of Physics Handbook, 2nd ed., section 6, p. 112 (1963).
16. S. M. Sze et al., Solid-State Electronics 7, 509 (1966).
17. Linus Pauling, The Nature of the Chemical Bond, (Cornell University Press, Ithaca, 1960), p. 93.
18. C. A. Mead, Appl. Phys. Letters 6, 103 (1965).
19. cf. K. R. Zanio et al., J. Appl. Phys. 39, 2818 (1968); K. K. Thornber and C. A. Mead, J. Phys. Chem. Solids 26, 1489 (1965); Wayne E. Tefft, J. Appl. Phys. 38, 5265 (1965).
20. K. Hecht, Z. Physik 77, 235 (1932).
21. S. Z. Weisz et al., J. Appl. Phys. 39, 2296 (1968).

22. A. S. Grove, Physics and Technology of Semiconductor Devices (John Wiley and Sons, New York, 1967), p. 131.

23. Heinz Fischer and Walter B. Ruppel, Applied Optics 3, 769 (1964).

24. Mark D. Tabak and Peter J. Warter, Jr., Phys. Rev. 173, 899 (1968).

25. Walter R. Beam, Electronics of Solids (McGraw-Hill, New York, 1965) p. 272.

26. Grove, ibid. p. 37.

27. Bateman Manuscript Project, Integral Transforms, Vol. 1 (McGraw-Hill, New York, 1954), p. 74. Eq. 2.4.26.

28. A. J. Bradley, Phil. Mag. 48, 477 (1924); M. Straumanis, Z. Krist. 102, 432 (1940).

29. W. J. Choyke and L. Patrick, Phys. Rev. 108, 25 (1957).

30. D. J. Olechna and R. S. Knox, Phys. Rev. 140, A986 (1965).

31. J. R. Reitz, Phys. Rev. 105, 1233 (1957).

32. A. von Hippel, J. Chem. Phys. 16, 372 (1948).

33. S. D. Coulson et al., J. Chem. Phys. 48, 2215 (1968).

34. cf. H. Kallman (ed.), Symposium on Electrical Conductivity in Organic Solids, (Interscience, New York, 1961).

35. Nelvin M. Saffren, Phys. Rev. 165, 870 (1968).

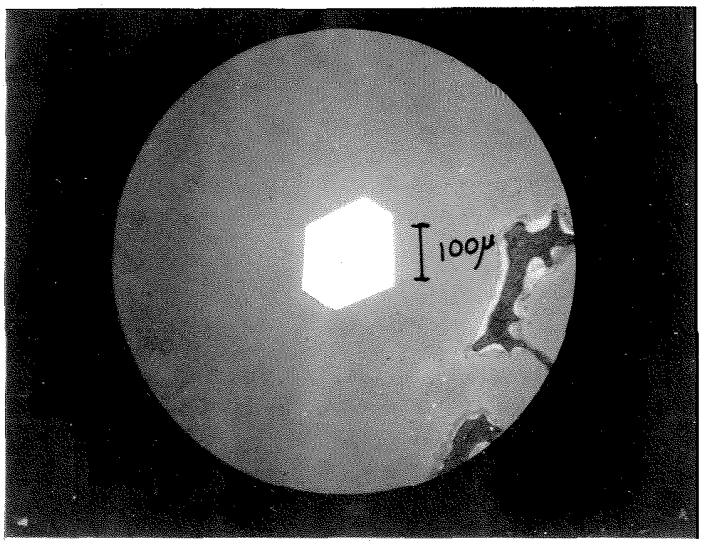

Figure 1. A typical crystal used in the transmission measurements. This crystal was about 1800 Å in thickness.

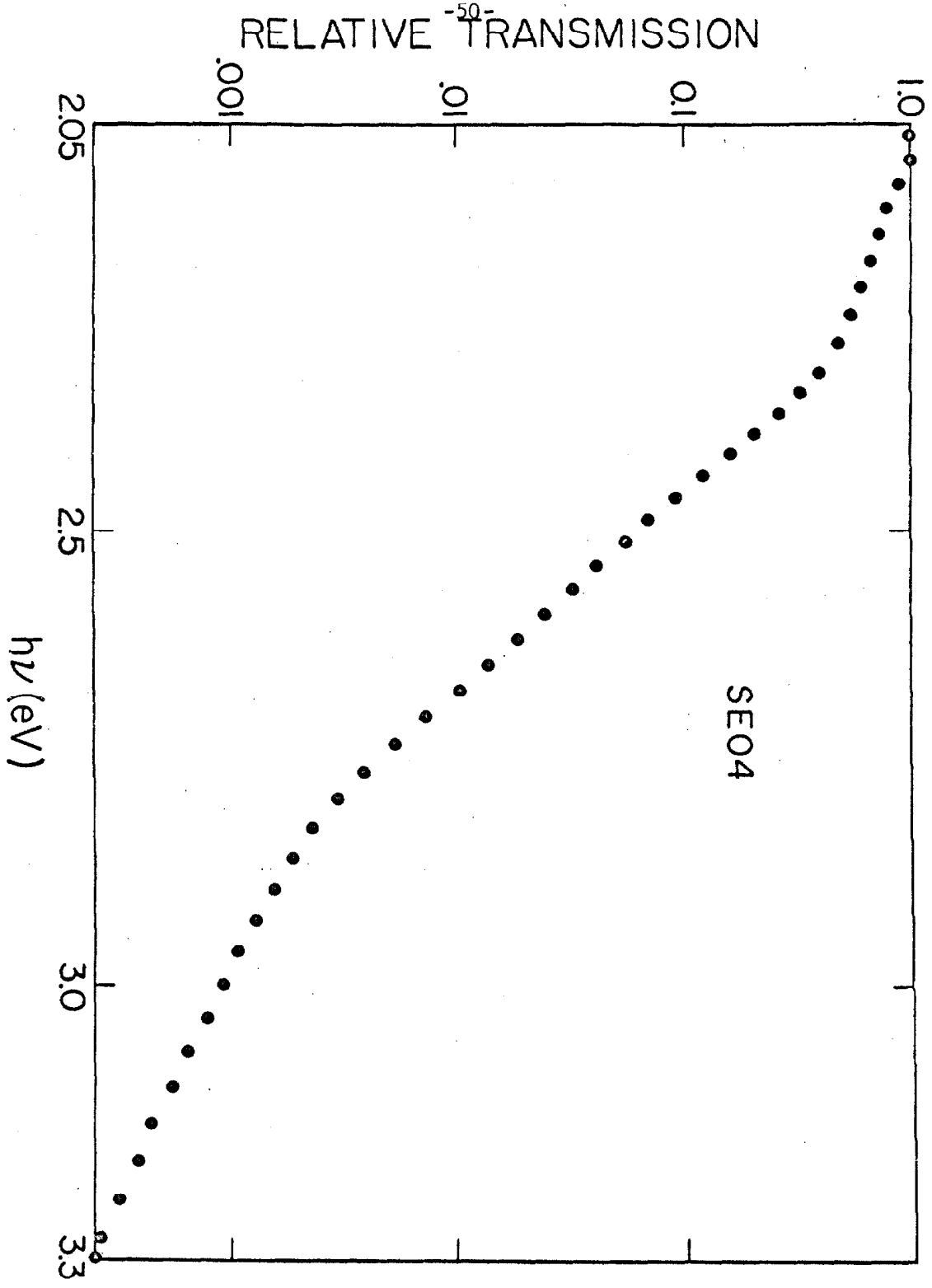

Figure 2. Relative transmission of a typical platelet of α-monoclinic Se.

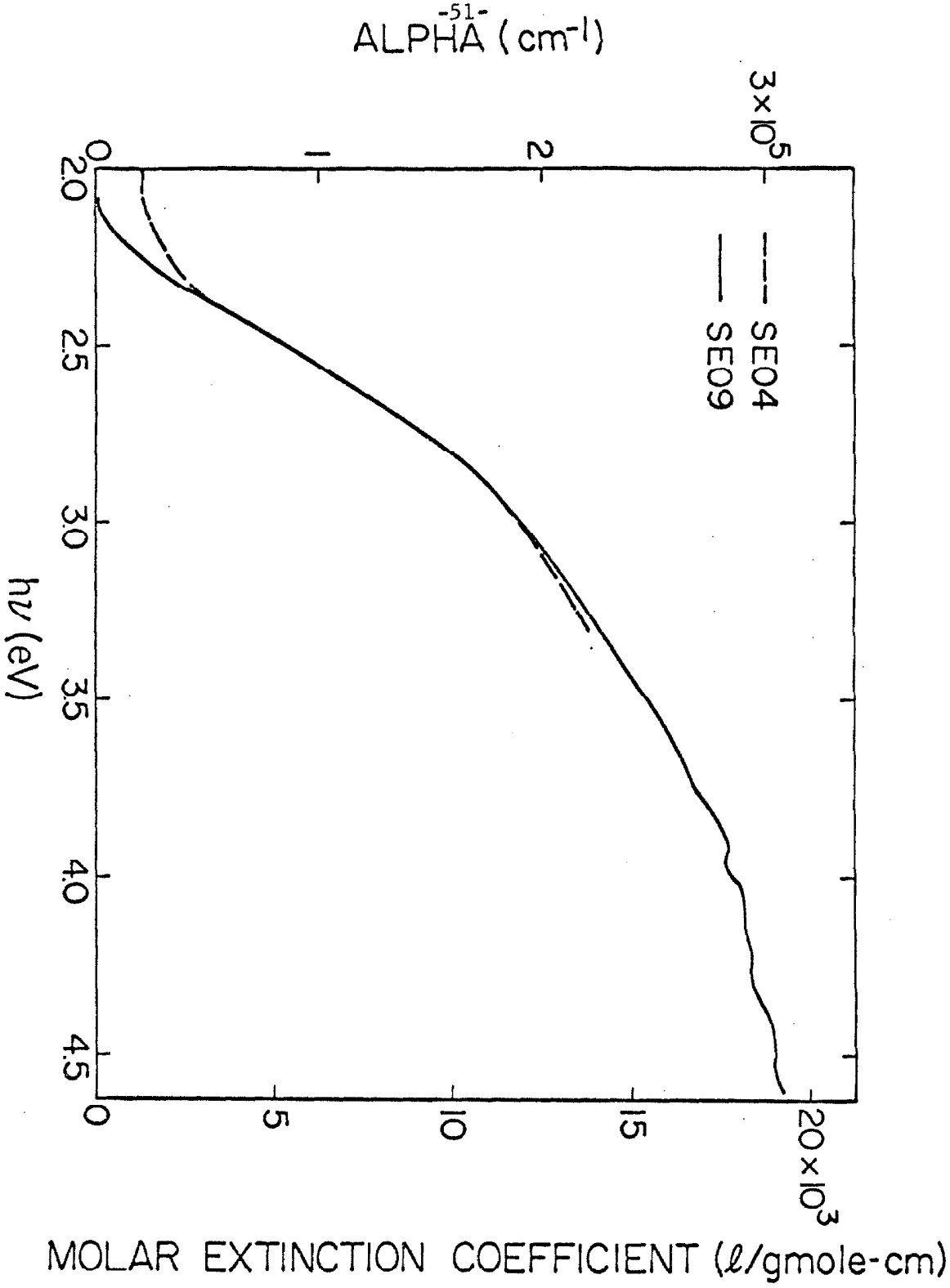

Figure 3. Normalized absorption of two α-monoclinic Se crystals. Se04 was 4102 Å ± 61 Å thick while Se09 was 1060 Å ± 48 Å thick.

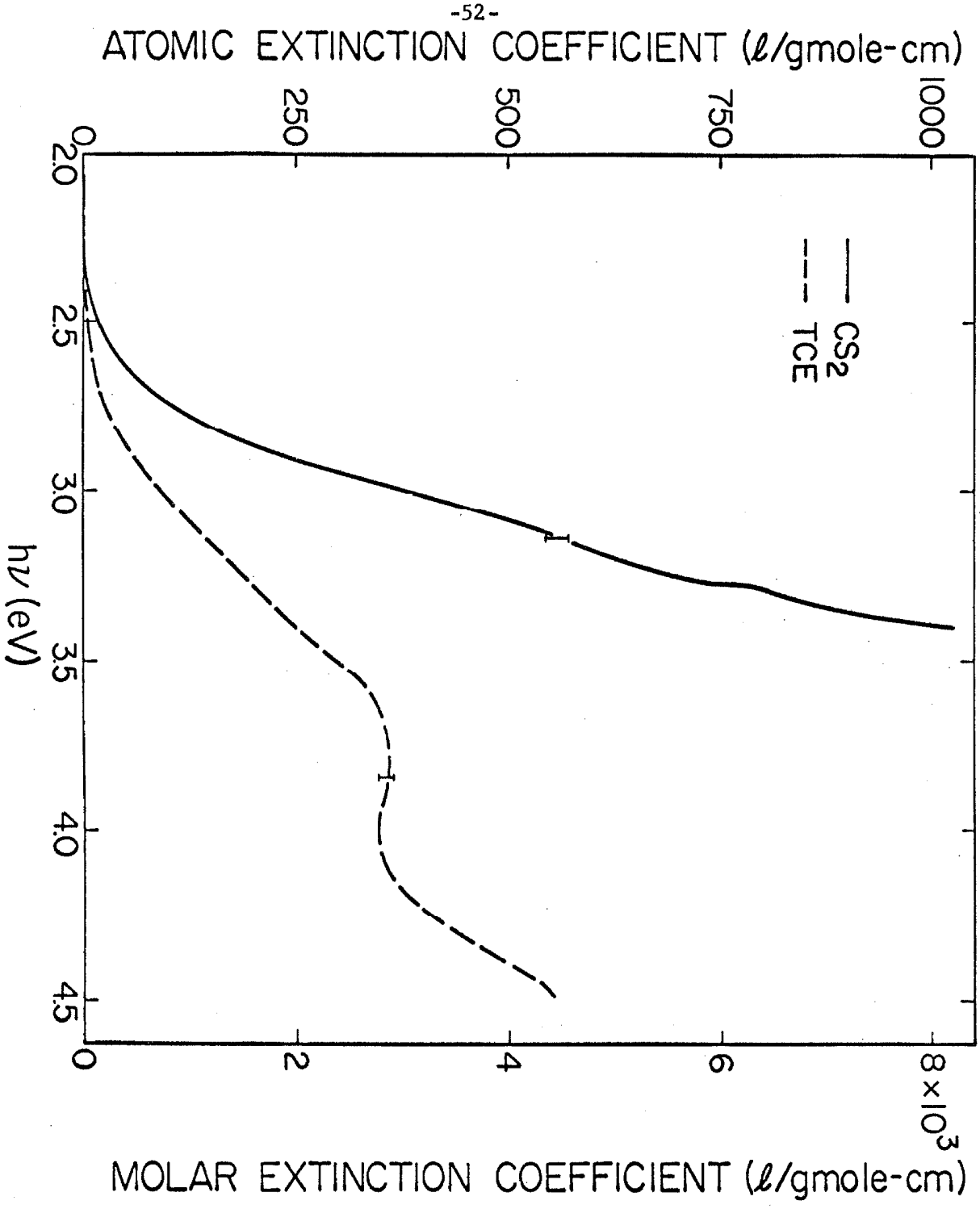

Figure 4. Extinction coefficient of selenium dissolved in CS_2 and trichlorethylene (TCE).

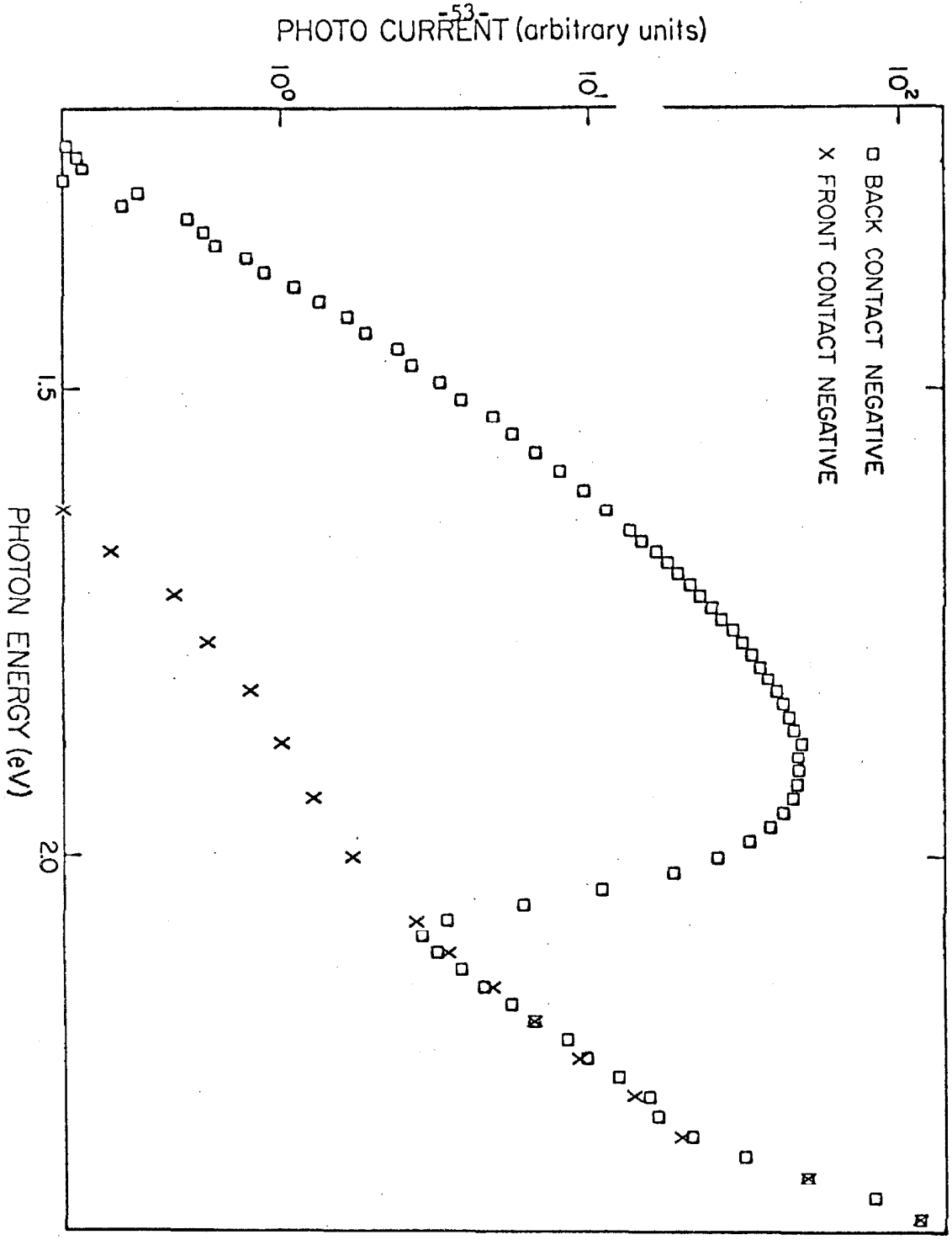

Figure 5. Photocurrent vs. photon energy for a Au-selenium-Au sample with large asymmetry in the area of the two gold contacts.

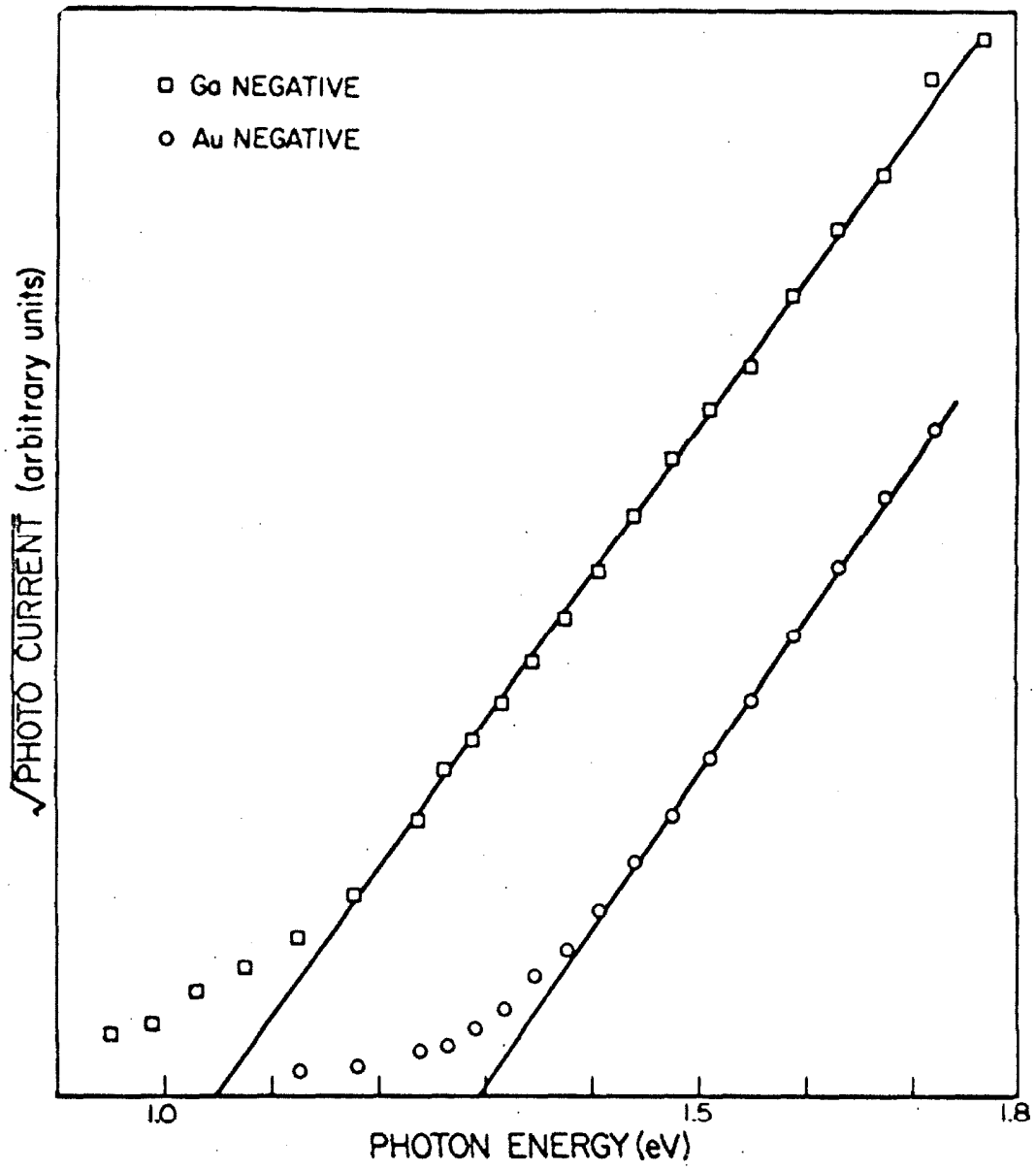

Figure 6. Square root of the photocurrent vs. photon energy for a Au-selenium-Ga sample.

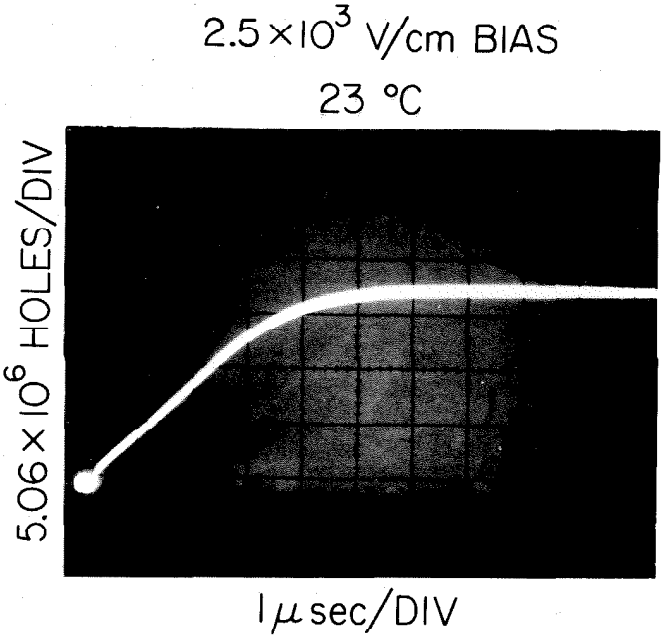

Figure 7. A typical oscillograph of the integrated drift current.

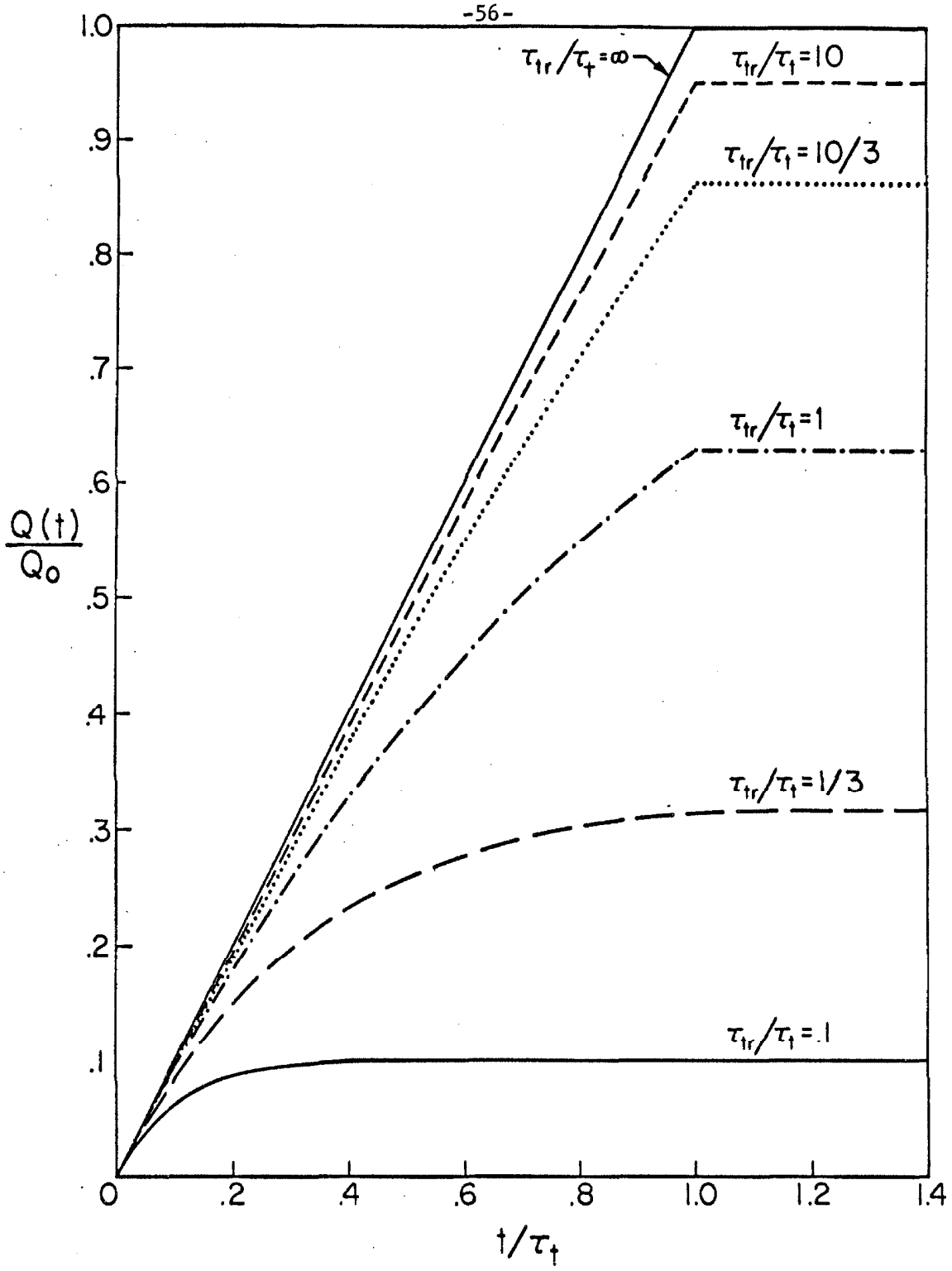

Figure 8. Theoretical curves for the integrated drift current with the ratio of the transit time to the trapping time as a parameter. These curves are for the case of deep traps where it is assumed that the trap release time is very much longer than the transit time.

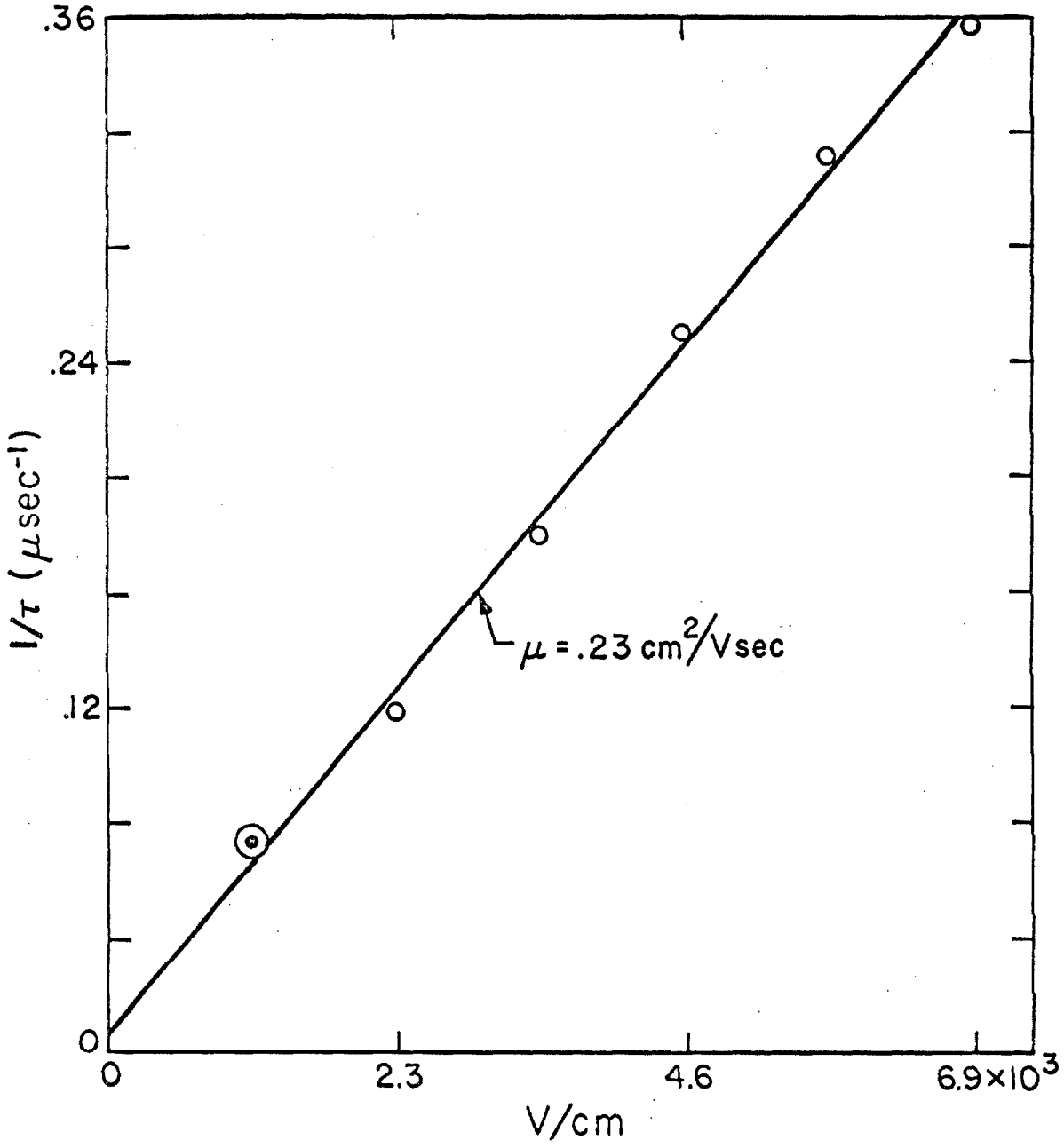

Figure 9. A typical plot of inverse transit time versus bias field. This particular plot is for holes at room temperature. The solid line represents a least-square fit of the data.

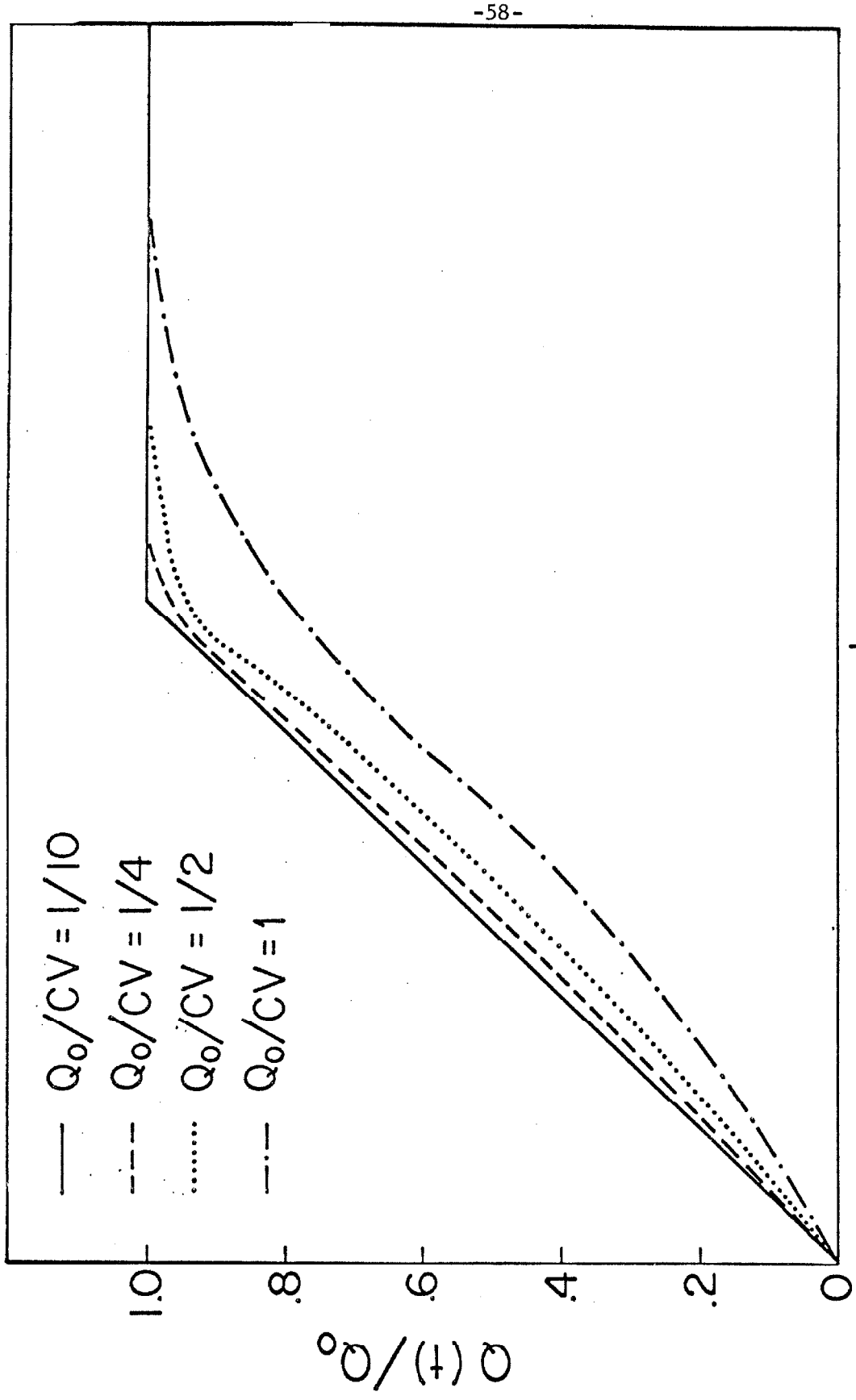

Figure 10. Theoretical curves for normalized transported charge versus time in the presence of space charge. The parameter Q_o/CV is a measure of the importance of space charge.

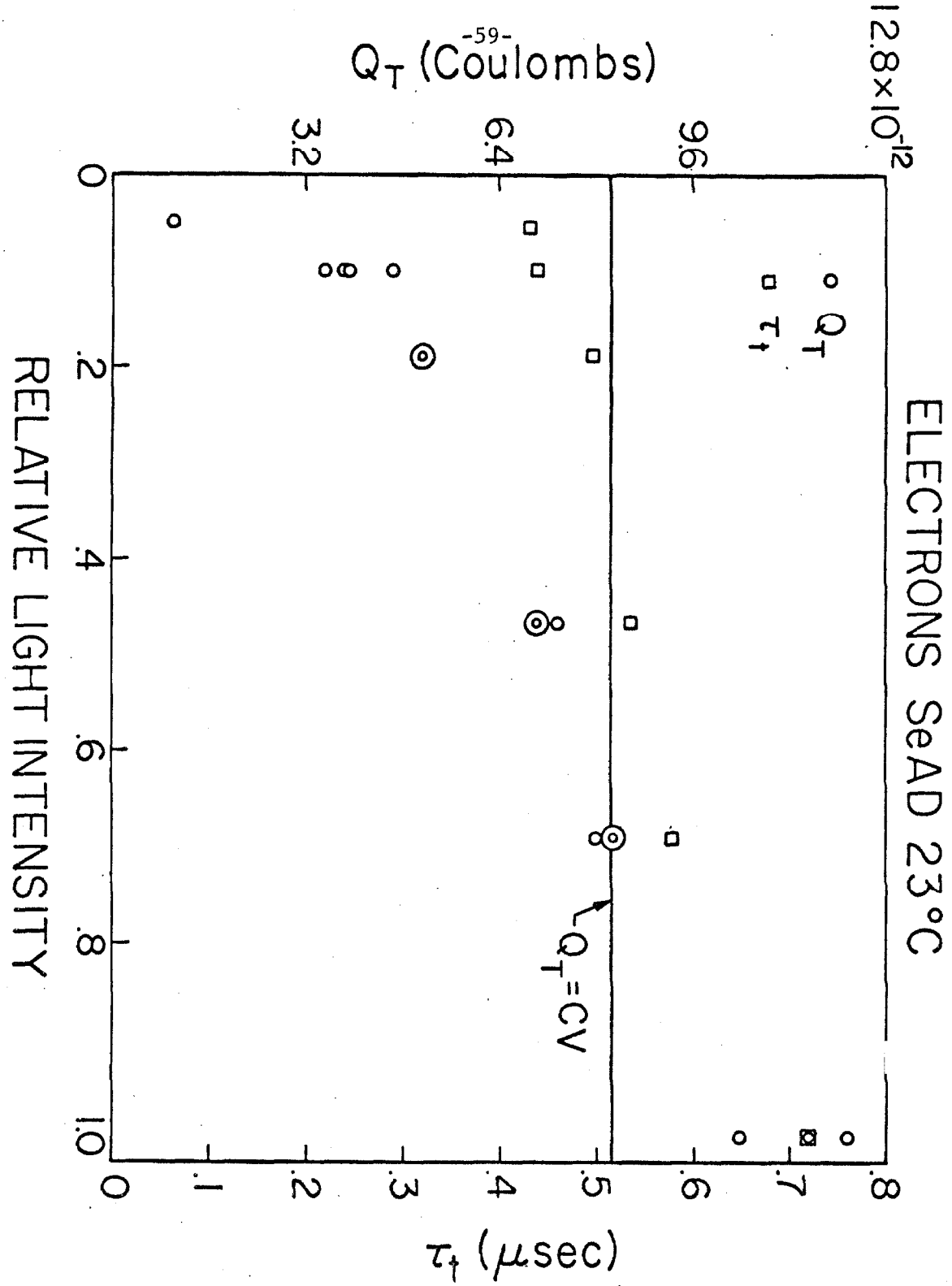

Figure 11. The figure shows the dependence of the total transported Q_t, and the transit time, τ_t, as a function of the relative intensity of the light which generates the carriers, in this case, electrons. These data were taken on sample SeAD at 23°C.

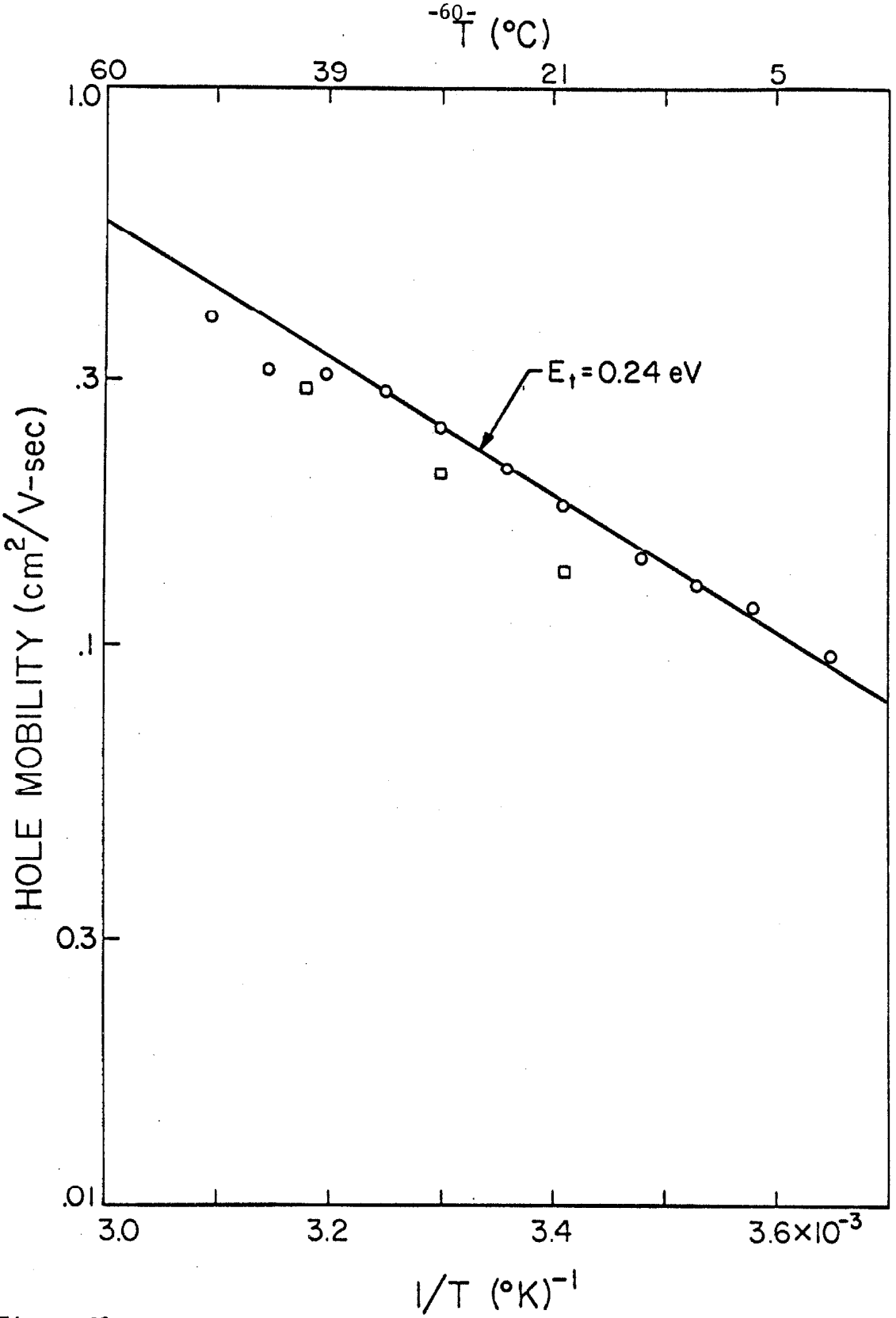

Figure 12. Logarithm of the hole mobility plotted vs. inverse temperature allows the depth, E_t, of the traps which control the mobility to be determined. The circles represent data taken going up in temperature (down in 1/T); while the squares represent data taken going down after having reached maximum temperature.

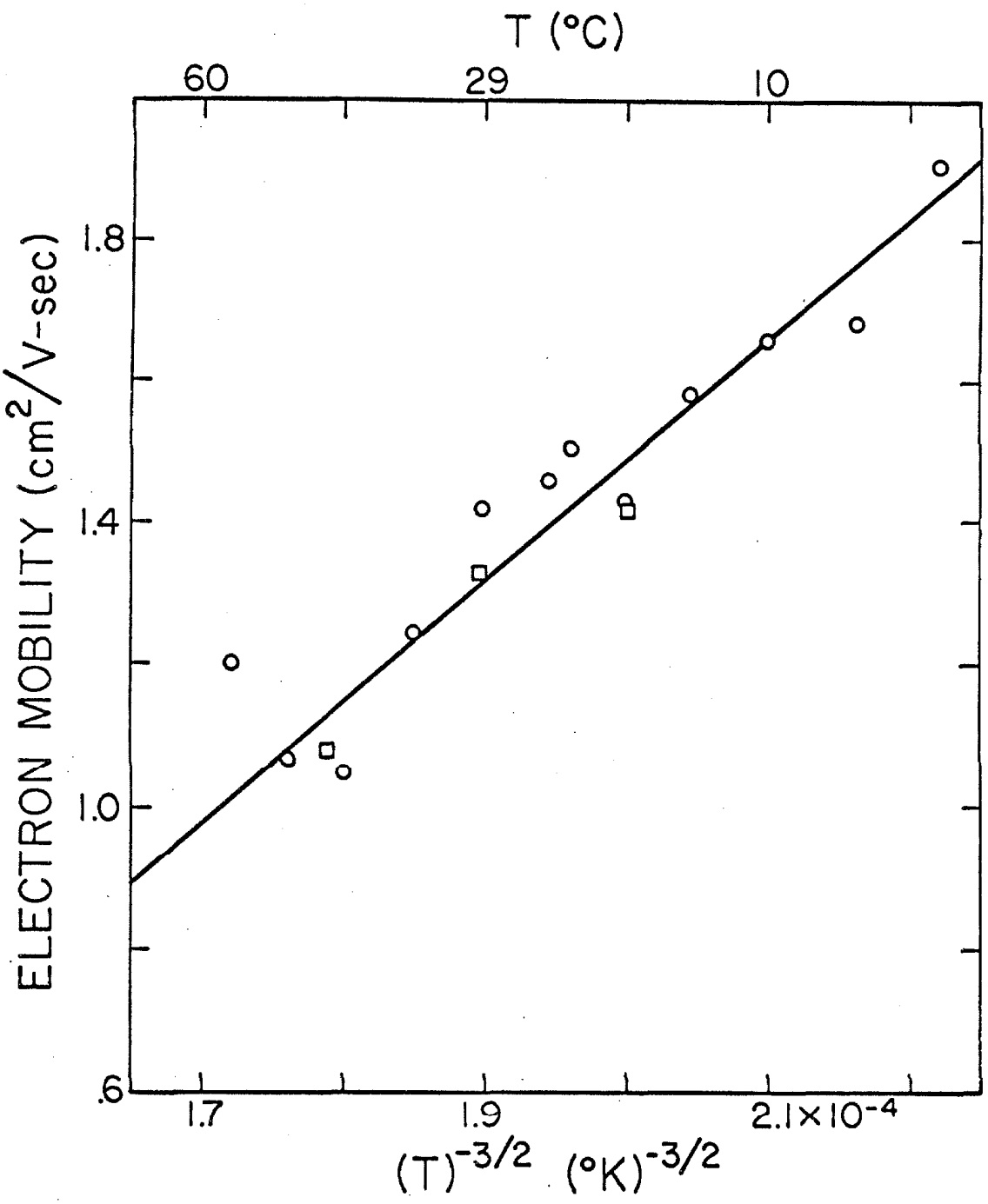

Figure 13. As is shown, the electron mobility varies linearly with $T^{-3/2}$. The circles represent data taken as the temperature was increased to maximum temperature (50°C) while the squares represent data taken as the temperature decreased after reaching the maximum.

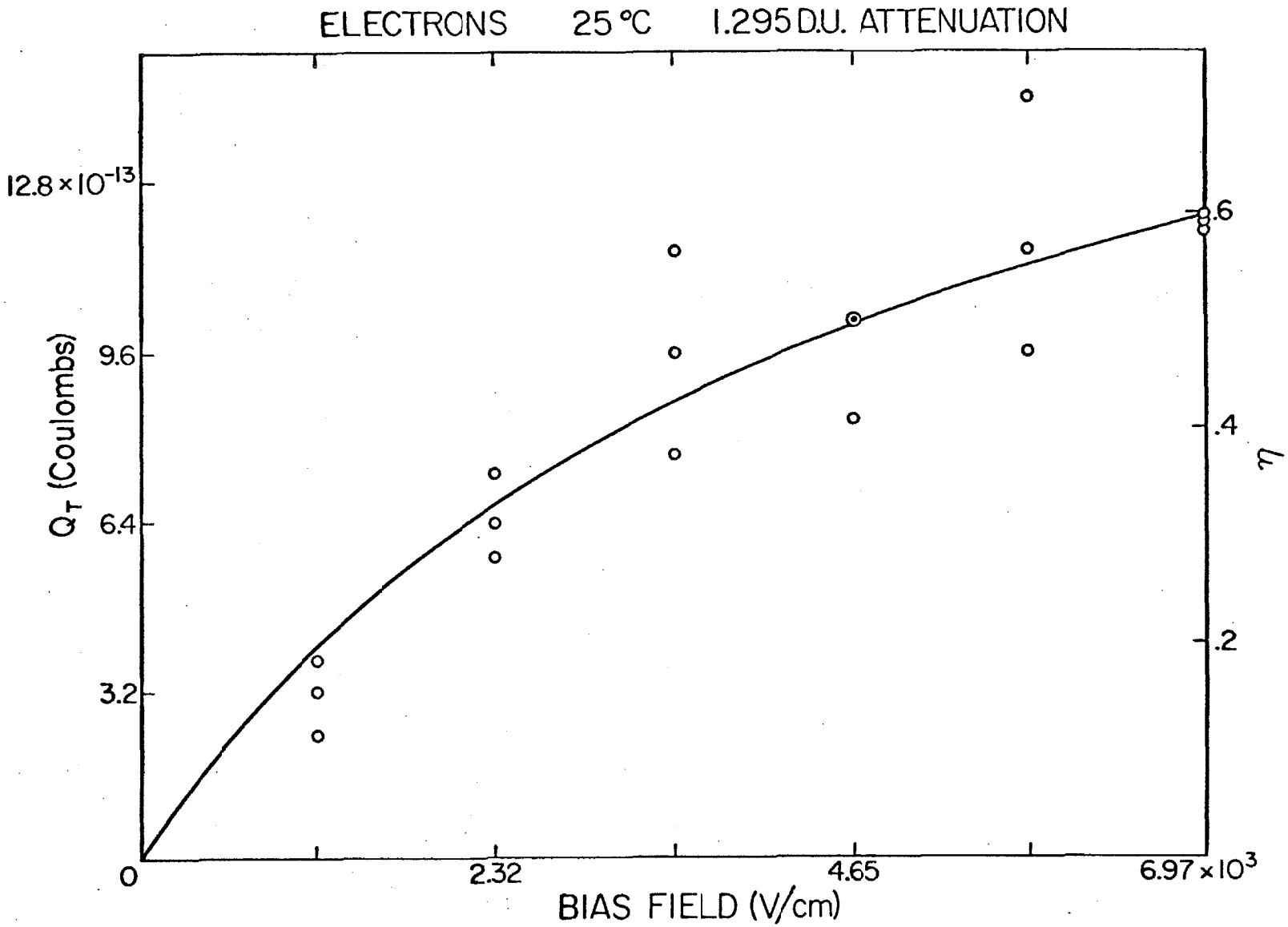

Figure 14. The data show the variation of the transported charge, Q_t, with field. The line is the theoretically predicted collection efficiency, η.

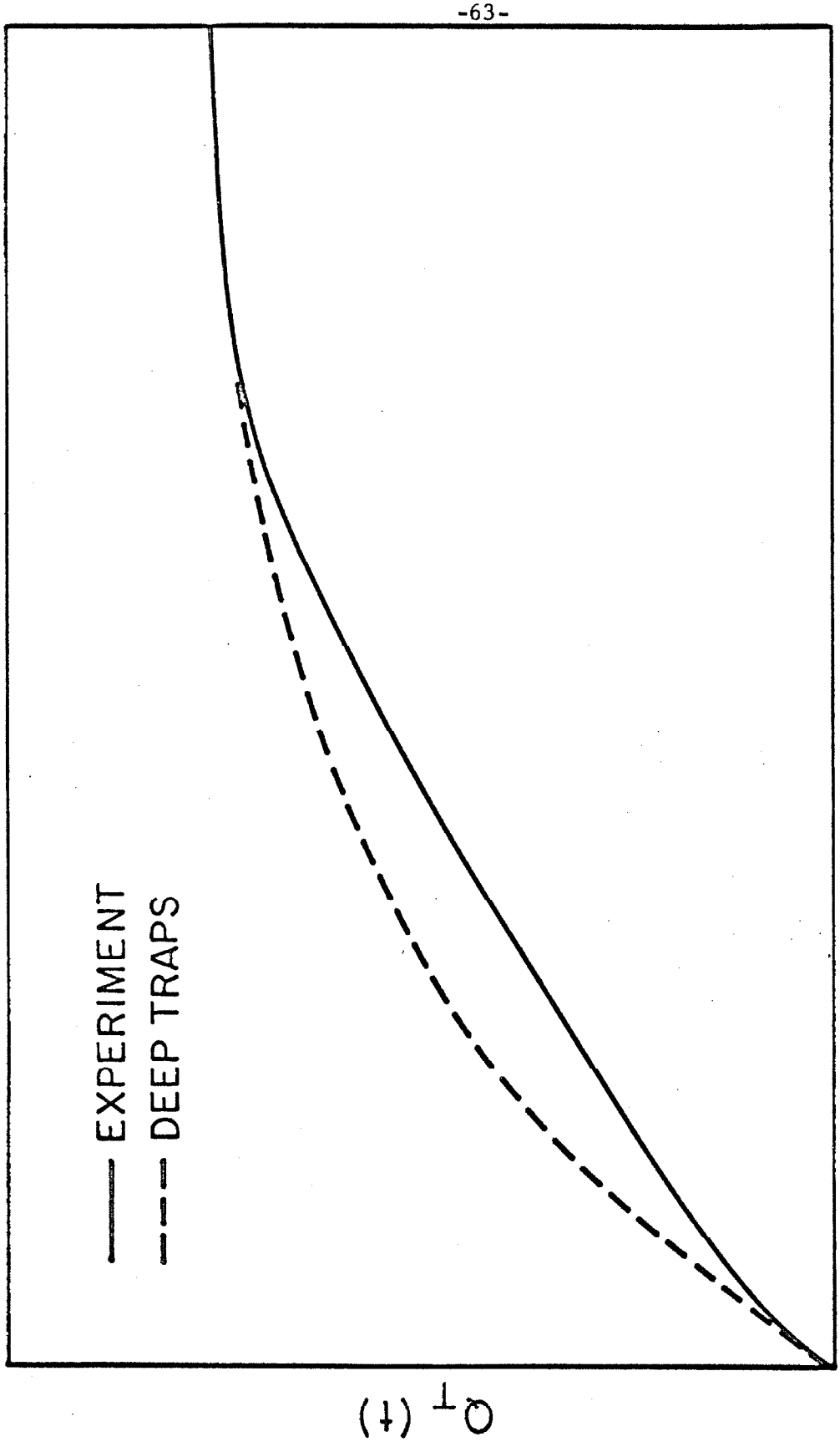

Figure 15. The solid line in this figure is a tracing of an oscillograph of Q(t) vs. t for the sample of figure 14 under 1160 V/cm bias. The dashed line is the curve which would be obtained if the field dependence of Q_T shown in fig. 14 were the result of deep trapping.

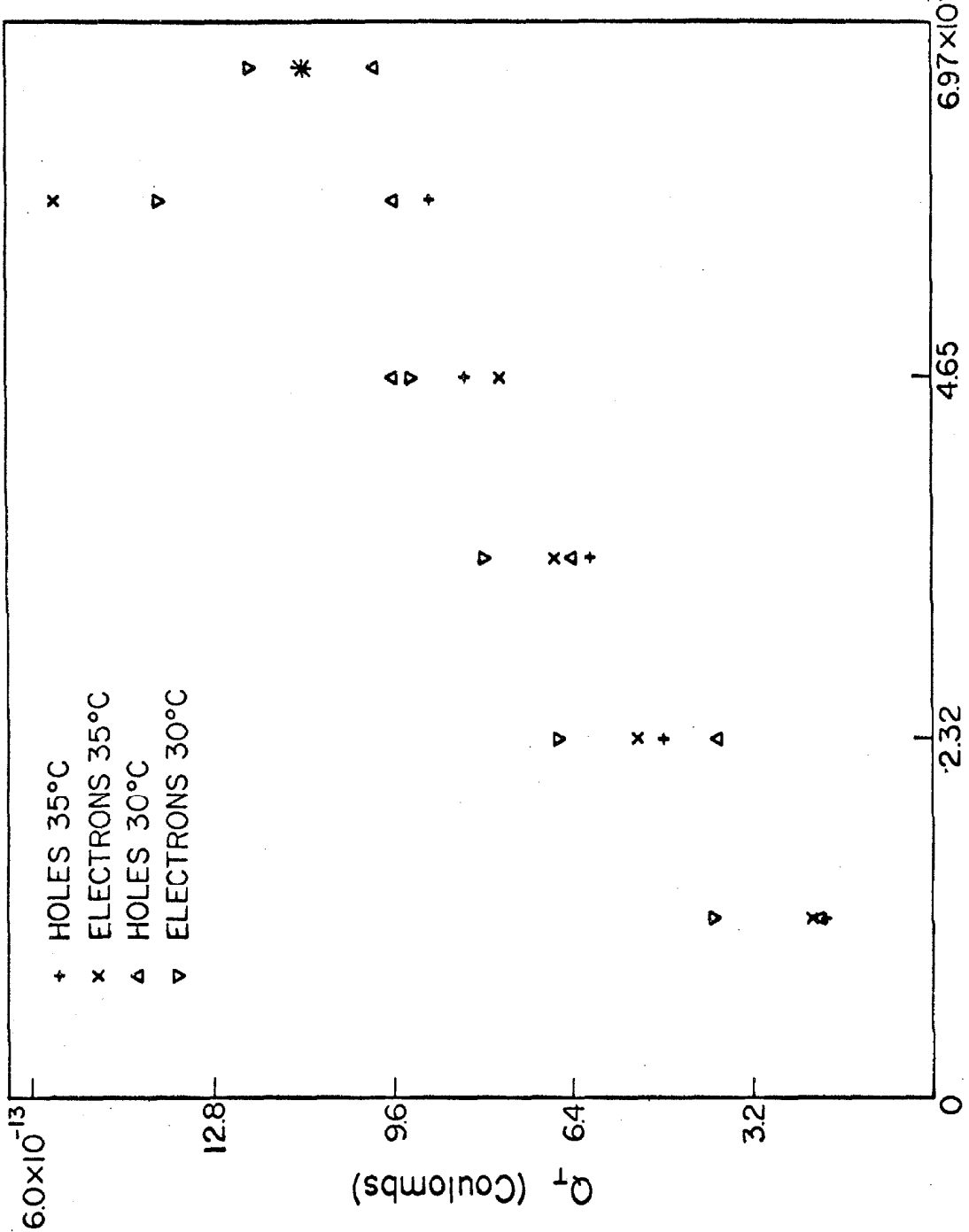

Figure 16. This figure demonstrates that Q_T is essentially independent of polarity of the carriers.

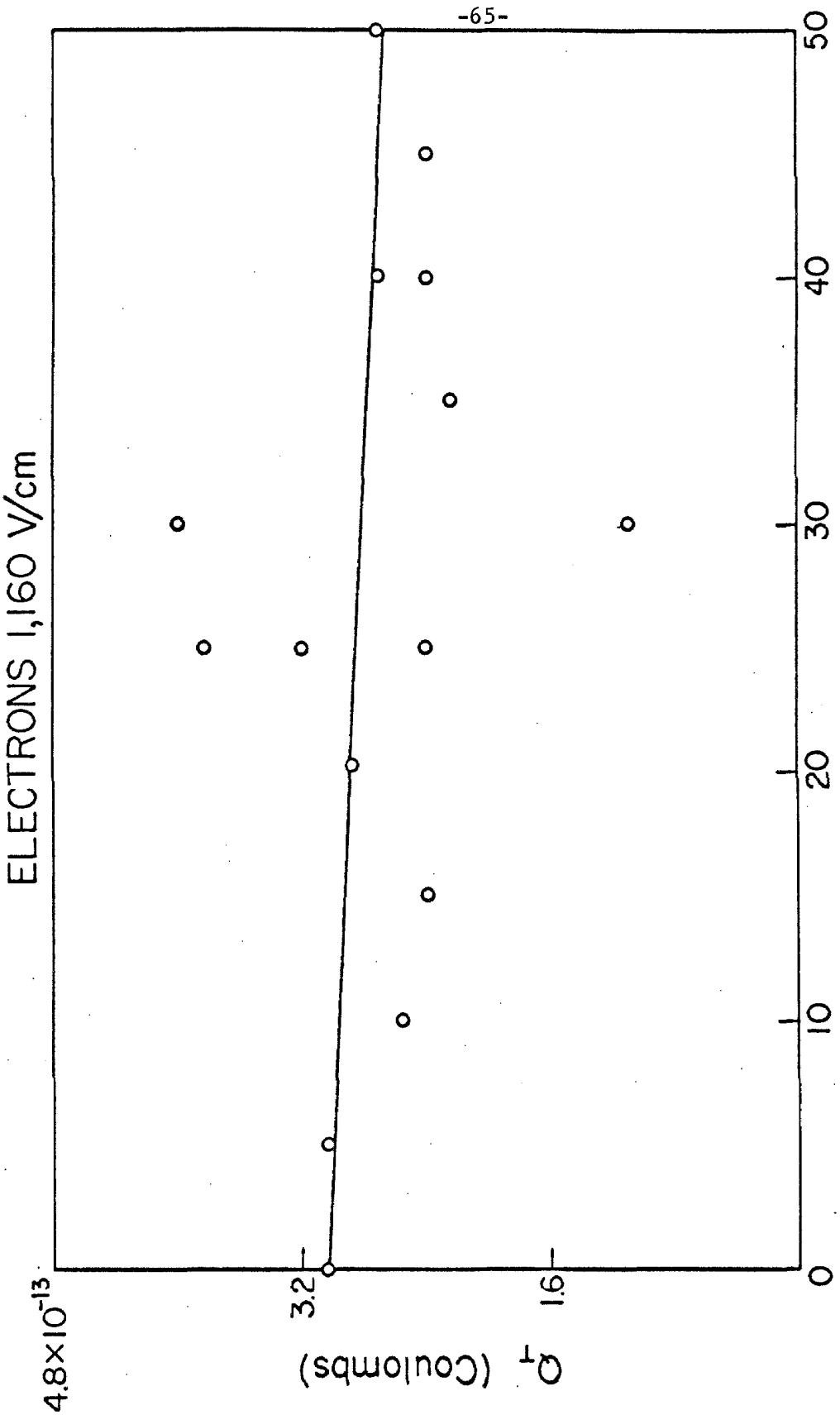

Figure 17. The data show the temperature variation of Q_t at a low value of field. The line is a least-squares, linear fit to the data.

List of Symbols

α	optical absorption constant
ϵ	extinction coefficient
d	sample thickness
μ	mobility
τ_t	transit time
τ_{tr}	trapping time
τ_R	trap release time
E	electric bias field
B	trapping rate per unit volume for empty trap
Q(t)	charge transferred across sample as function of time
Q_o	total charge of one sign generated by light flash
Q_T	total charge transferred across sample
f	probability a trap is occupied by an electron
f'	probability a trap is occupied by a hole
E_t	energy separating trapping level from conduction level
V	applied bias voltage
n(x,t)	carrier density
q	magnitude of charge on an electron
T	temperature
k	Boltzmann's constant
η	collection efficiency
A	area of contact
F	μE